# Simulated responses of soil carbon to climate change in CMIP6 Earth System Models: the role of false priming

Rebecca M. Varney[1, 3], Sarah E. Chadburn[1], Simon Jones[1, 3], Eleanor J. Burke[2], Andy J. Wiltshire[2, 3], and Peter M. Cox[1, 3]

[1]Department of Mathematics and Statistics, Faculty of Environment, Science and Economy, University of Exeter, Laver Building, North Park Road, Exeter, EX4 4QE, UK
[2]Met Office Hadley Centre, FitzRoy Road, Exeter, EX1 3PB, UK
[3]Global Systems Institute, University of Exeter, Laver Building, North Park Road, Exeter, EX4 4QE, UK

**Correspondence:** Rebecca M. Varney (r.varney@exeter.ac.uk)

**Abstract.** Reliable estimates of soil carbon change are required to determine the carbon budgets consistent with the Paris Agreement climate targets. This study evaluates projections of soil carbon during the 21$^{st}$ century in CMIP6 Earth System Models (ESMs) under a range of atmospheric composition scenarios. In general, we find a reduced spread of changes in global soil carbon ($\Delta C_s$) in CMIP6 compared to the previous CMIP5 model generation. However, similar reductions were not

5   seen in the derived contributions to $\Delta C_s$ due to both increases in plant Net Primary Productivity (NPP, named $\Delta C_{s,NPP}$) and reductions in the effective soil carbon turnover time ($\tau_s$, named $\Delta C_{s,\tau}$). Instead, we find a strong relationship across the CMIP6 models between these NPP and $\tau_s$ components of $\Delta C_s$, with more positive values of $\Delta C_{s,NPP}$ being correlated with more negative values of $\Delta C_{s,\tau}$. We show that the concept of 'false priming' is likely to be contributing to this emergent relationship, which leads to a decrease in the effective soil carbon turnover time as a direct result of NPP increase and occurs when the rate

10   of increase of NPP is relatively fast compared to the slower timescales of a multipool soil carbon model. This finding suggests that the structure of soil carbon models within ESMs in CMIP6 has likely contributed towards the reduction in the overall model spread in future soil carbon projections since CMIP5.

## 1   Introduction

The response of soil carbon to human-induced climate change represents one of the greatest uncertainties in determining future

15   atmospheric $CO_2$ concentrations (Canadell et al., 2021). Global soil carbon stocks contain at least 3 times more carbon than present atmospheric concentrations and is the largest store of carbon on the land surface of Earth (Jackson et al., 2017). The land surface has been a carbon sink throughout the 20$^{th}$ century and is estimated to be absorbing about 30% of current $CO_2$ emissions (Friedlingstein et al., 2022). However, the long-term response of soil carbon is uncertain due to large stocks which are known to be particularly sensitive to changes in $CO_2$ and the subsequent global warming (Cox et al., 2000). For example,

20   permafrost thaw under climate change has the potential to release significant amounts of carbon into the atmosphere over a short period of time with increased warming, representing a significant feedback within the climate system (Schuur et al., 2022;

Hugelius et al., 2020; Burke et al., 2017). Therefore, quantifying the future response of soil carbon under future changes to climate is vital in determining the long-term potential land carbon storage.

Soil carbon storage in the future will be determined by the net response of changes in land-atmosphere carbon exchange under increased anthropogenic $CO_2$. The carbon fluxes which control the fate of global soil carbon stocks are known to be sensitive to changes in climate, and therefore result in soil carbon driven feedbacks to climate change (Canadell et al., 2021). The overall effect of climate change on soil carbon is not very well constrained due to competing feedbacks (Arora et al., 2020, 2013). These include both the negative feedback due to the $CO_2$ fertilisation effect resulting in increased absorption of carbon by the land surface (Schimel et al., 2015), and the positive climate feedback due to increased carbon losses via soil respiration (Crowther et al., 2016; Van Gestel et al., 2018). The balance between these effects will determine the future response of soil carbon stocks under a changing climate (Friedlingstein et al., 2006).

This study assumes Net Primary Productivity (NPP) represents the input flux of carbon to the system, and is defined as the net rate of accumulation of carbon by vegetation arising from photosynthesis minus the loss from plant respiratory fluxes (Todd-Brown et al., 2014, 2013). In the absence of nutrient and moisture limitations (Wieder et al., 2015b; Green et al., 2019), NPP is projected to increase under increased atmospheric $CO_2$ due to the $CO_2$ fertilisation effect, which can result in an increased soil carbon storage through increased litter (Schimel et al., 2015). Heterotrophic respiration ($R_h$) is assumed to represent the output flux of carbon from the soil and is defined as the carbon losses due to decomposition from microbes in the soil. $R_h$ is projected to increase under global warming, due to an increased rate of microbial decomposition under warming (Varney et al., 2020), in the absence of significant increases in soil moisture (Sierra et al., 2015; Schmidt et al., 2011). Soil carbon turnover time ($\tau_s$) is defined as the ratio of soil carbon stocks to the output flux of carbon ($R_h$). Global warming alone generally reduces $\tau_s$ resulting in carbon residing in the soil for less time and a release of carbon from the soil into the atmosphere (Crowther et al., 2016). The effective soil carbon turnover time can also reduce under increasing litterfall inputs (e.g. due to $CO_2$ fertilisation of plant growth), because the faster components of the soil increase more quickly than the slower components. The net effect of this is that a higher fraction of the soil carbon flux is cycled in the fast pools under increasing litterfall, which reduces the effective soil carbon turnover time - a transient phenomenon known as false priming (Koven et al., 2015).

In this study, CMIP6 Earth System Models (ESMs) are used to predict changes to soil carbon stocks under future climate scenarios with differing magnitudes of climate change (*SSP126*, *SSP245*, *SSP585*; Eyring et al. (2016); O'Neill et al. (2016)). The aim is to evaluate estimates of soil carbon change ($\Delta C_s$) during the 21st century to: (a) quantify the soil carbon driven feedback to climate change, and (b) enable comparisons with the previous generation of CMIP5 ESMs (*RCP2.6*, *RCP4.5*, *RCP8.5*; Taylor et al. (2012); Meinshausen et al. (2011)). Additionally, this study includes analysis of 21st century carbon fluxes to and from the soil, represented by changes in NPP and $\tau_s$, and investigates how these individual terms contribute to the net soil carbon response projected by ESMs. Finally, a simple box model is used to investigate soil carbon change, along with idealised simulations (C4MIP) which separately model the physiological and climate effects of increasing atmospheric $CO_2$. Our aim is to distinguish more clearly between the direct and indirect mechanisms of reduced soil carbon turnover times by isolating the effects of false priming in models.

## 2   Methods

### 2.1   Earth system models

#### 2.1.1   Future climate scenarios

This study uses output data from 10 CMIP6 ESMs (Eyring et al., 2016): ACCESS-ESM1-5, BCC-CSM2-MR, CanESM5,
CESM2, CNRM-ESM2-1, IPSL-CM6A-LR, MIROC-ES2L, MPI-ESM1-2-LR, NorESM2-LM, and UKESM1-0-LL. For comparison between the CMIP generations, output data from 9 CMIP5 ESMs are also used (Taylor et al., 2012): BNU-ESM,
CanESM2, GFDL-ESM2G, GISS-E2-R, HadGEM2-ES, IPSL-CM5A-LR, MIROC-ESM, MPI-ESM-LR, and NorESM1-M.
The ESMs included were chosen due to the availability of the data required at the time of analysis (CMIP6: https://esgf-node.llnl.gov/search/cmip6/, last access: 8 April 2022) and CMIP5: (https://esgf-node.llnl.gov/search/cmip5/, last access: 12
April 2022).

The use of CMIP allows for comparison between ESMs in the different ensemble generations. Table 1 presents key soil
carbon ESM information from both CMIP6 and CMIP5 (adapted from Tables 1 and 2 in Varney et al. (2022)). The Table can be used to identify key ESM updates between CMIP6 and CMIP5, such as: the simulation of interactive nitrogen
in CMIP6 (ACCESS-ESM1.5, CESM2, MIROC-ES2L, MPI-ESM1.2-LR, NorESM2-LM and UKESM1-0-LL) compared to
CMIP5 (NorESM1-M) and the number of soil carbon pools (dead carbon pools). The ESMs where both CMIP5 and CMIP6
generations are included in our analysis are: CanESM2 and CanESM5, GFDL-ESM2G and GDFL-ESM4, IPSL-CM5A-LR
and IPSL-CM6A-LR, MIROC-ESM and MIROC-ES2L, MPI-ESM-LR and MPI-ESM1.2-LR, NorESM1-M and NorESM2-LM, and HadGEM2-ES and UKESM1-0-LL, respectively, where direct comparisons can be made. It is noted that some Land
Surface Models within ESMs share similarities (e.g. CESM2 and NorESM2-LM both use the Community Land Model version
5; Arora et al. (2020)).

Within ESMs, specific soil carbon processes are modelled using biogeochemical models which are used to simulate the flow
and storage of carbon within the soil. Since early models, both the litter and soil are simulated using separate carbon pools,
which are used to represent differing sensitivities of carbon to decomposition. The allocation of carbon into pools is often
dependent on the molecular structure of the litter and the long-term stability (Exbrayat et al., 2013). Early examples of soil
carbon models are the grass and agroecosystems dynamic model (CENTURY; Parton et al. (1988)) and the Rothamsted carbon
model (ROTH-C; Jenkinson et al. (1991)). Updated variants of these models are still widely used to represent soil carbon
decomposition in modern ESMs within CMIP (Arora et al., 2020; Todd-Brown et al., 2018). Table 1 presents the number of
soil carbon pools (dead carbon pools) within both CMIP5 and CMIP6 ESMs, which can be used to compare between the ESMs.

The analysis in this study considers 3 future climate scenarios defined by CMIP, which are used to consider different levels
of global warming and associated climate policies. The CMIP6 Shared Socioeconomic Pathways (SSPs) considered in this
study are: *SSP126*, *SSP245*, *SSP585*, which run from 2015 to 2100 (O'Neill et al., 2014; O'Neill et al., 2016). These pathways
are chosen to allow for comparison with the CMIP5 Representative Concentration Pathways (RCPs): *RCP2.6*, *RCP4.5* and
*RCP8.5*, which run from 2005 to 2100 (Meinshausen et al., 2011). It is noted that the SSP and RCP concentration scenarios

are not identical, but they are similar enough to enable helpful comparisons between CMIP5 and CMIP6 projections. For the reference period from which change is calculated, the CMIP *Historical* simulation was considered, where the simulation runs from 1850 to 2005 in CMIP5 and from 1850 to 2015 in CMIP6. A change ($\Delta$) was defined as the difference between the last decade of the 21$^{st}$ century (time-averaged between 2090 and 2100) and the last decade of the CMIP5 historical simulation (time-averaged between 1995-2005), which allows for consistency between the CMIP generations. If a timeseries is considered, the historical reference period (historical simulation time-averaged between 1995-2005) was subtracted from the entire future climate simulation (e.g. *SSP126* minus the historical reference period).

### 2.1.2   C4MIP experiments

This study also uses model experiments set up by the Coupled Climate-Carbon Cycle Model Intercomparison Project (C4MIP), which are idealised experiments designed to separate the effects of $CO_2$ increases and associated climate changes on land and ocean carbon stores. In these experiments additional effects such as land-use change, aerosols or non-$CO_2$ greenhouse gases are not included, and nitrogen deposition is fixed at pre-industrial values (Jones et al., 2016). The use of these experiments allows for a more focused evaluation of soil carbon and related fluxes by isolating sensitivities to $CO_2$ and associated climate changes (e.g. global temperature changes), as well as removing additional complications in the SSP simulations. The experiments included are: (1) a '*full* 1% $CO_2$ simulation' (CMIP6 simulation *1pctCO2*), which is a simulation that sees a 1% increase in atmospheric $CO_2$ per year, starting from pre-industrial concentrations (285 ppm) and running for 150 years (*full* 1% $CO_2$), (2) a biogeochemically coupled '*BGC* simulation' (CMIP6 simulation *1pctCO2-bgc*), where the 1% $CO_2$ increase per year only affects the carbon cycle component of the ESM and the radiative code remains at pre-industrial $CO_2$ values ($CO_2$ only), and (3) a radiatively coupled '*RAD* simulation' (CMIP6 simulation *1pctCO2-rad*), where the 1% $CO_2$ increase per year affects only the radiative code and the carbon cycle component on the ESM remains at pre-industrial $CO_2$ values (climate only). These simulations are used with 10 CMIP6 ESMs for further analysis: ACCESS-ESM1-5, BCC-CSM2-MR, CanESM5, CESM2, GFDL-ESM4, IPSL-CM6A-LR, MIROC-ES2L, MPI-ESM1-2-LR, NorESM2-LM, and UKESM1-0-LL, and here 2x$CO_2$ and 4x$CO_2$ are defined as 70 and 140 years into the simulations, respectively.

### 2.1.3   Climate variables

Using ESM output variables, soil carbon ($C_s$) is defined as the sum of carbon stored in soils and surface litter (CMIP variable *cSoil* + CMIP variable *cLitter*). This allows for a more consistent comparison between the models due to differences in how soil carbon and litter carbon are defined. For models that do not report a separate litter carbon pool (*cLitter*), soil carbon is taken to be simply the *cSoil* variable (UKESM1-0-LL in CMIP6, GISS-E2-R and HadGEM2-ES in CMIP5). Spatial $C_s$ is given in units of kg m$^{-2}$, and global total $C_s$ is given in units of PgC, which are calculated using an area weighted sum (using the model land surface fraction, CMIP variable *sftlf*).

Additionally, ESM output variables were used to define the soil carbon driven climate feedbacks. Net Primary Productivity (NPP, CMIP variable *npp*) is defined as the net carbon assimilated by plants via photosynthesis minus loss due to plant respiration and is used to represent the net carbon input flux to the system. Heterotrophic Respiration ($R_h$, CMIP variable *rh*) is

defined as the microbial respiration within global soils and is used to define an effective global soil carbon turnover time ($\tau_s$), see Equation 1. $\tau_s$ (years) is defined as the ratio of mean soil carbon to annual mean heterotrophic respiration (where the mean represents an area weighted global average). Carbon fluxes (NPP and $R_h$) are considered as area weighted global totals in units of PgC yr$^{-1}$.

$$\tau_s = \frac{C_s}{R_h} \tag{1}$$

## 2.2 Breaking down the projected changes in soil carbon

From Equation 1, soil carbon ($C_s$) can be defined as shown by Equation 2. Future soil carbon stocks can be defined as initial soil carbon ($C_{s,0}$) plus a change in soil carbon ($\Delta C_s$), as shown by Equation 3, where the subscript 0 denotes the initial state (historical simulation time-averaged between 1995-2005). Equation 3 can be expanded to give Equation 4, which can be simplified to give Equation 5.

$$C_s = R_h \tau_s \tag{2}$$

$$C_{s,0} + \Delta C_s = (R_{h,0} + \Delta R_h)(\tau_{s,0} + \Delta \tau_s) \tag{3}$$

$$C_{s,0} + \Delta C_s = R_{h,0}\tau_{s,0} + \tau_{s,0}\Delta R_h + R_{h,0}\Delta \tau_s + \Delta R_h \Delta \tau_s \tag{4}$$

$$\Delta C_s = \tau_{s,0}\Delta R_h + R_{h,0}\Delta \tau_s + \Delta R_h \Delta \tau_s \tag{5}$$

To isolate the above and below ground effects on soil carbon, the separate effects due to changes in NPP and changes due to $\tau_s$ are considered (Todd-Brown et al., 2014). For carbon to be conserved however, the difference between the global fluxes NPP and $R_h$ in a transient climate must be taken into account, where the difference is defined as the Net Ecosystem Productivity (NEP), as shown in Equation 6.

$$\text{NEP} = \text{NPP} - \text{R}_h \tag{6}$$

Equation 6 can be substituted into Equation 5, to obtain an equation for $\Delta C_s$ in terms of NPP, NEP and $\tau_s$ (Equation 7).

$$\Delta C_s = \tau_{s,0}\Delta(\text{NPP} - \text{NEP}) + (\text{NPP}_0 - \text{NEP}_0)\Delta \tau_\text{s} + \Delta(\text{NPP} - \text{NEP})\Delta \tau_\text{s} \tag{7}$$

If the initial state is a steady-state, the initial NEP ($\text{NEP}_0$) will be approximately equal to zero. However, as our initial state is defined as the end of the historical simulation, $\text{NEP}_0$ will therefore be non-zero as a result of the contemporary global land carbon sink. ESMs may also include additional carbon fluxes that cause changes to the resultant soil carbon inputs, such as: grazing, harvest, land-use change, and fire (Todd-Brown et al., 2014). The $\Delta\text{NEP}$ terms in Equation 7 implicitly includes these effects.

Finally, Equation 7 can be expanded to give Equation 8, and the individual responses which make up the total change in soil carbon ($\Delta C_s$) can be broken-down into 6 components:

$$\Delta C_s = \tau_{s,0}\Delta\text{NPP} - \tau_{s,0}\Delta\text{NEP} + \text{NPP}_0\Delta\tau_s - \text{NEP}_0\Delta\tau_s + \Delta\text{NPP}\Delta\tau_s - \Delta\text{NEP}\Delta\tau_s \tag{8}$$

Equation 7 is exact for given time-varying values of NPP, NEP and $\tau_s$. The individual terms in Equation 8 are defined as given below.

$$\Delta C_{s,NPP} \approx \tau_{s,0}\Delta\text{NPP} \tag{9}$$

$$\Delta C_{s,NEP} \approx -\tau_{s,0}\Delta\text{NEP} \tag{10}$$

$$\Delta C_{s,\tau} \approx \text{NPP}_0\Delta\tau_s \tag{11}$$

$$\Delta C_{s,\tau_{NEP}} \approx -\text{NEP}_0\Delta\tau_s \tag{12}$$

Where, $\Delta C_{s,NPP}$ is the change in soil carbon due to changes in NPP, $\Delta C_{s,NEP}$ is the change in soil carbon due to changes in NEP, and $\Delta C_{s,\tau}$ is the change in soil carbon due to changes in $\tau_s$ (with $\Delta C_{s,\tau_{NEP}}$ accounting for non-equilibrium). The two additional terms are: the non-linear term between NPP and $\tau_s$ ($\Delta\text{NPP}\Delta\tau_s$) and the non-linear term between NEP and $\tau_s$ ($\Delta\text{NEP}\Delta\tau_s$).

## 3 Results and Discussion

### 3.1 Projected changes in soil carbon

A reduced spread in projected end of 21st century estimates of $\Delta C_s$ is seen in CMIP6 compared to CMIP5 (Fig. 1). This reduced spread is shown in Fig. 1, where projections of $\Delta C_s$ by 2100 in CMIP6 are compared with those from CMIP5 across

the different future scenarios. The reduced range of projected changes is seen across all future scenarios (*SSP126* and *RCP2.6*, *SSP245* and *RCP4.5*, *SSP585* and *RCP8.5*), with the range in CMIP6 consistently less than 50% of the equivalent range in CMIP5 (Fig. 1). The standard deviation of projections about the ensemble mean $\Delta C_s$ is also reduced in CMIP6 compared with CMIP5 by 50%, consistent across all future climate scenarios (Tables 2 and A1, bottom rows). It is noted that the large

170 range in CMIP5 estimates is mostly a result of large increases in $C_s$ in HadGEM2-ES and MPI-ESM-LR, together with the large $C_s$ losses in GISS-E2-R (Fig. 1). An updated CMIP6 version of the GISS-E2-R model is not included in this analysis of this study, which could contribute to the reduced uncertainty from CMIP5. However, the updated equivalent CMIP6 models UKESM1-0-LL (from HadGEM2-ES) and MPI-ESM1-2-LR (from MPI-ESM-LR) have projected estimates of $\Delta C_s$ which are more consistent with the other models in the CMIP6 ensemble.

175  Nearly all of the ESM projections in CMIP6 suggest an increase in $C_s$ by 2100, however CMIP5 models project both increases (positive $\Delta C_s$) and decreases (negative $\Delta C_s$) in soil carbon during the 21st century (Fig. 1). In CMIP5 projections, the future responses of soil carbon range from an increase of 23.2% (HadGEM2-ES) to a decrease of 6.50% (GISS-E2-R) in *RCP8.5*, where across all future scenarios approximately half of the models show increases and half show decreases in $\Delta C_s$ (Table A1). In CMIP6, the future responses of soil carbon range from an increase of 12.5% (MPI-ESM1-2-LR) to a decrease of

180 2.25% (ACCESS-ESM1.5) in *SSP585*, however the majority of models predict an increase in $\Delta C_s$ across all future scenarios (Table 2).

  Despite more consistent projections of increased $\Delta C_s$ in CMIP6 compared with CMIP5, it is apparent that greater $CO_2$ forcing (i.e. *SSP585* compared with *SSP126*) does not always imply a greater magnitude of increased $C_s$. In contrast to what is seen in CMIP6, the majority of CMIP5 models project an increased magnitude in estimated $\Delta C_s$ with increased $CO_2$

185 forcing (Fig. 1). In CMIP6, half the models (CESM2, CNRM-ESM2-1, IPSL-CM6A-LR, NorESM2-LM, and UKESM1-0-LL) estimate less soil carbon accumulation by 2100 (i.e. a smaller increase or a greater decrease) in *SSP585* when compared with *SSP126*. This effect is most prominent in BCC-CSM2-MR and UKESM1-0-LL, where a turning point from increasing to decreasing soil carbon is seen in the mid-century of the *SSP585* projections (Fig. 2). This is opposed to an estimated increase in soil carbon storage with increased forcing, which is generally seen in CMIP5 and the remaining CMIP6 models (CanESM5,

190 MIROC-ES2L, and MPI-ESM1-2-LR). This finding is likely due to a saturation of the $CO_2$ fertilisation effect, compared with no saturation of increased respiration with warming in these ESMs. This finding suggests a potential limit to $\Delta C_s$ increase and a reduced likelihood of a carbon sink under more extreme levels of climate change.

  The spatial pattern of estimated $\Delta C_s$ (Fig. 3) is quite variable between CMIP6 ESMs. For example in the tropical regions, where increases in soil carbon can be seen in 6 of the CMIP6 ESMs (BCC-CSM2-MR, CanESM5, CESM2, MIROC-ES2L,

195 and NorESM2-LM), but decreases are seen in the remaining 4 (ACCESS-ESM1-5, CNRM-ESM2-1, IPSL-CM6A-LR, and UKESM1-0-LL). There is a lack of agreement in the high northern latitudes amongst the CMIP6 ESMs (Fig. 3), where it is known that the uncertainty surrounding the fate of soil carbon stocks in these regions is particularly important due to the large magnitude of carbon stored (Burke et al., 2020; Jackson et al., 2017). It has previously been found that a high accumulation of northern latitude $C_s$ is predicted amongst CMIP5 ESMs, however this $C_s$ response has not been suggested in empirical studies

200 based on observational findings (Todd-Brown et al., 2014). The results here suggest that this accumulation (increased $\Delta C_s$)

remains in the majority of CMIP6 ESMs (Fig. 3), although reductions in northern latitude soil carbon stocks were found in 3 CMIP6 ESMs (BCC-CSM2-MR, CESM2 and NorESM2-LM, with BCC-CSM2-MR seeing reductions in a greater area). These ESMs which predicted northern latitude $C_s$ reductions were previously found to simulate historical northern latitude soil carbon stocks which are more consistent with the observational estimates seen in these regions (Varney et al., 2022).

## 3.2 Future changes to land-atmosphere fluxes

The projected $\Delta C_s$ is a result of the changing input and output land-atmosphere fluxes under climate change. To a first order, the response of soil carbon will be determined by changes to NPP and to $\tau_s$ (see Equation 7). In this section, future projections of these fluxes are analysed in both CMIP6 and CMIP5 ESMs.

### 3.2.1 Net Primary Productivity

NPP is projected by CMIP6 ESMs to increase during the 21$^{\text{st}}$ century, with a greater increase with increasing climate forcing (across SSP scenarios). This result is consistent with the projections of $\Delta$NPP amongst the CMIP5 models (Fig. 4; Todd-Brown et al. (2014)). Projections amongst ESMs however, show disagreement in the magnitude of $\Delta$NPP by 2100 across all future climate scenarios, where a projected CMIP6 ensemble increase of $24.6 \pm 16.9$ PgC yr$^{-1}$ is seen in *SSP585*. The largest projections of $\Delta$NPP amongst the CMIP6 models are seen in CanESM5 and BCC-CSM2-MR, where increases of 65.8 PgC yr$^{-1}$ (47% increase) and 39.4 PgC yr$^{-1}$ (43% increase) are projected by 2100 under *SSP585*, respectively. This is compared to ACCESS-ESM1-5 which has the lowest projected changes amongst the CMIP6 models with an increase of only 4.07 PgC yr$^{-1}$ (10% increase) by 2100 under *SSP585* (Table 3).

The CMIP6 ensemble sees a slightly increased range in end of century $\Delta$NPP compared with CMIP5, across all future scenarios (Tables 3 and A2). Fig. 4 suggests that the increased range is mostly due to outlying projections of $\Delta$NPP (CanESM5), where greater increases are seen compared to the majority of models within the ensemble. It is noted that a cluster of ESMs which have similar projections of $\Delta$NPP is seen within CMIP6 (CESM2, MIROC-ES2L, MPI-ESM1-2-LR, NorESM2-LM, and UKESM1-0-LL). The cluster is found to be made up of ESMs which include the simulation of an interactive nitrogen cycle (shown by the dashed lines throughout this study), which is a common addition within CMIP6 ESMs (ACCESS-ESM1.5, CESM2, MIROC-ES2L, MPI-ESM1-2-LR, NorESM2-LM and UKESM1-0-LL; Davies-Barnard et al. (2020)). ACCESS-ESM1-5 is the only model within CMIP6 which simulates interactive nitrogen, but does not predict similar $\Delta$NPP to the other nitrogen ESMs in CMIP6. However, the projections of $\Delta$NPP in ACCESS-ESM1-5 are similar to the projections of NorESM1-M in CMIP5, which is the only CMIP5 model considered here to simulate interactive nitrogen (Table 1).

### 3.2.2 Soil carbon turnover time

Future $\tau_s$ is projected by CMIP6 ESMs to decrease by 2100 across all future SSP scenarios (Fig. 5). A greater reduction in $\tau_s$ is seen with increased climate forcing scenario, where a reduced $\tau_s$ is a faster soil carbon turnover time, and implies that carbon is cycled back to the atmosphere in less time due to an increased carbon output from the soil (increased $R_h$, see Equation 1).

This result is consistent with the projections of $\Delta\tau_s$ amongst the CMIP5 models (Fig. 5; Todd-Brown et al. (2014)). However, it is found that greater variation exists amongst the CMIP6 ESMs end of century estimates, where a projected CMIP6 ensemble $\Delta\tau_s$ value of -7.65 $\pm$ 5.65 years is seen in *SSP585* compared to -6.13 $\pm$ 3.03 years for CMIP5 ESMs in *RCP8.5* (Tables 3 and A2).

The CMIP6 ESMs with the greatest reductions in effective global $\tau_s$ by 2100 is seen in BCC-CSM2-MR, CESM2 and NorESM2-LM, where global carbon turnover in the soil is at least 14 years faster at the end of the *SSP585* simulation compared to the start of the 21$^{st}$ century (historical reference). The CMIP6 models with the least change in effective global $\tau_s$ are ACCESS-ESM1-5, IPSL-CM6A-LR, and MPI-ESM1-2-LR, where global carbon turnover in the soil is only around 2 years faster at the end of the *SSP585* simulation (Table 3). The increased range in CMIP6 from CMIP5 is primarily due to the large $\tau_s$ reductions seen in the CMIP6 models NorESM2-LM, CESM2 and BCC-CSM2-MR (Fig. 5).

### 3.3 Breaking down the projected changes in soil carbon

To understand the projected end of century changes in soil carbon storage ($\Delta C_s$) in ESMs, the individual responses of soil carbon due to changes in NPP ($\Delta C_{s,NPP}$, see Equation 9) and the response due to changes in $\tau_s$ ($\Delta C_{s,\tau}$, see Equation 12) were diagnosed for both CMIP5 and CMIP6 as shown in Fig. 6. Future $\Delta C_s$ (blue bars) is found to be mostly a result of the net effect of the linear terms: $\Delta C_{s,NPP}$ (dark green bars) and $\Delta C_{s,\tau}$ (red bars). However, there are also non-negligible contributions from the non-linear term: $\Delta NPP\Delta\tau_s$ (black bars), and a small addition due to the non-equilibrium terms: $\Delta C_{s,NEP}$ (light green bars), $\Delta C_{s,\tau_{NEP}}$ (pink bars), and $\Delta NEP\Delta\tau_s$ (grey bars).

The importance of investigating the individual processes which contribute to the net $\Delta C_s$ in ESMs can be seen (Fig. 6). In Fig. 6 it is seen that the net $\Delta C_s$ is relatively small compared to the individual changes from the derived components, where especially large magnitudes are seen in the increased $C_s$ due to increased $\Delta NPP$ ($\Delta C_{s,NPP}$) and the decreased $C_s$ due to reduced $\Delta\tau_s$ ($\Delta C_{s,\tau}$). For example, in *SSP585* there is a range of approximately 170 PgC in net $\Delta C_s$, from an increase of 132 PgC (CNRM-ESM2-1) to a reduction of 35 PgC (BCC-CSM2-MR). However, the $\Delta C_{s,NPP}$ contribution has a much larger range of 1442 PgC, from an increase of 95 PgC (ACCESS-ESM1-5) to an increase of 1517 PgC (NorESM2-LM). Similarly, $\Delta C_{s,\tau}$ has a range of 756 PgC, from a decrease of 115 PgC (ACCESS-ESM1-5) to a decrease of 871 PgC (NorESM2-LM).

The magnitude of change seen from the individual feedbacks ($\Delta C_{s,NPP}$ and $\Delta C_{s,\tau}$) is not obviously related to the resultant magnitude of soil carbon change (Fig. A1). For example, NorESM2-LM projects large $\Delta C_{s,NPP}$ and $\Delta C_{s,\tau}$ values (1517 PgC and -871 PgC in *SSP585*, respectively), however a relatively small net change in soil carbon (49 PgC in *SSP585*). Conversely, CNRM-ESM2-1 projects smaller $\Delta C_{s,NPP}$ and $\Delta C_{s,\tau}$ values (667 PgC and -413 PgC in *SSP585*, respectively), but a larger net soil carbon change (132 PgC in *SSP585*). Within ESMs, it is found that the change in soil carbon is determined by the relationship between all the contributing terms to the net $\Delta C_s$ response, as opposed to the absolute size of a given contribution (Fig. 6).

Surprisingly, a very strong correlation is found amongst the ESMs in CMIP6 (r$^2$ value of 0.97) between the linear terms $\Delta C_{s,NPP}$ and $\Delta C_{s,\tau}$ (Fig. 7(a)). This leads to the partial cancelling of the terms, with a relatively small resultant net $\Delta C_s$. When comparing with the CMIP5 ensemble, a lower correlation between $\Delta C_{s,NPP}$ and $\Delta C_{s,\tau}$ is seen (r$^2$ value of 0.084, Fig.

7(a)). This correlation amongst CMIP6 ESMs results in net $\Delta C_s$ being more clustered in CMIP6 compared to CMIP5 (Fig. 1), despite a similarly large variation in the individual contributions (Fig. 6). The strong CMIP6 correlation ($r^2 = 0.97$) remains when the fractional changes ($\Delta C_{s,NPP}/C_{s,0}$ and $\Delta C_{s,\tau_{NPP}}/C_{s,0}$, where $C_{s,0}$ is initial soil carbon stocks) are plotted instead (Fig. 7(b)).

Fig. 6 also shows that the differences in ESM projections of $\Delta C_s$ are partly due to differing magnitudes of the non-linear term ($\Delta \text{NPP} \Delta \tau_s$). A linear assumption is commonly used which would allow these cross-terms to be neglected ($\Delta \text{NPP}/\text{NPP} << 1$ and $\Delta \tau_s / \tau_s << 1$; Koven et al. (2015)). However, the ESM projected magnitudes of $\Delta \text{NPP} \Delta \tau_s$ are found to be relatively large, especially in the more extreme climate scenarios (Fig. 6). In *SSP585*, a range from a decreased $C_s$ of 11 PgC (ACCESS-ESM1-5) to a decreased $C_s$ of 599 PgC (BCC-CSM2-MR) is found amongst the CMIP6 models due to only the $\Delta \text{NPP} \Delta \tau_s$ term, and in some cases values greater magnitudes are seen than the net $\Delta C_s$ (BCC-CSM2-MR, CanESM5, CESM2, NorESM2-LM, and UKESM1-0-LL). The term is greater when there are large and counteracting magnitudes of $\Delta \text{NPP}$ and $\Delta \tau_s$, which results in a non-negligible product.

Additionally, to obtain the overall change in soil carbon seen in the models, contributions from the non-equilibrium terms ($\Delta C_{s,NEP}$, $\Delta C_{s,\tau_{NEP}}$, and $\Delta \text{NEP} \Delta \tau_s$) must also be included (Fig. 6). The $\Delta C_{s,NEP}$ term represents the change in soil carbon due to the net carbon sink during the 21$^{\text{st}}$ century, which exists while the climate is in a transient state due to continuous climate change. By definition, the magnitude of $\Delta C_{s,NEP}$ is negative if $\Delta \text{NEP}$ is positive, which implies a greatest or faster increase in NPP with respect to $R_h$ seen in the majority of ESMs. The contribution from these terms is found to be relatively small in most models, but not in all. In *SSP585*, projections of $\Delta C_{s,NEP}$ amongst CMIP6 models range from a reduction of 333 PgC (NorESM2-LM) to a gain of 8.74 PgC (ACCESS-ESM1-5). In CMIP5, exceptions where greater $\Delta C_{s,NEP}$ terms are found in the GISS-E2-R and MPI-ESM-LR models, implying the models are far from equilibrium at the end of the 21$^{\text{st}}$ century. The change in soil carbon due to the change in NEP ($\Delta C_{s,NEP}$) is often found to be greater in the models which see greater magnitudes of $\Delta C_{s,NPP}$ and $\Delta C_{s,\tau}$.

### 3.4 Investigating the emergent relationship between $\Delta C_{s,NPP}$ and $\Delta C_{s,\tau}$

In this subsection, the emergent relationship between $\Delta C_{s,NPP}$ and $\Delta C_{s,\tau}$ present across the CMIP6 ensemble is investigated using the idealised C4MIP simulations (see Methods). This enables investigation of the apparent negative correlation without additional complex processes which are included in the SSP simulations. By isolating the sensitivities to $CO_2$ and climate, we can more easily identify the processes which results in the apparent coupling between NPP and soil carbon turnover time in CMIP6 ESMs. Fig. 8 presents the relationship between $\Delta C_{s,NPP}$ and $\Delta C_{s,\tau}$ for each CMIP6 ESMs as in Fig. 7, but for the *full* 1% $CO_2$, *BGC* ($CO_2$ only), and *RAD* (climate only) simulations. It is found that $\Delta C_{s,NPP}$ and $\Delta C_{s,\tau}$ are strongly correlated in the *full* 1% $CO_2$ simulation, at both 2x$CO_2$ ($r^2$ value of 0.925) and 4x$CO_2$ ($r^2$ value of 0.839). The correlation is found to remain in the *BGC* simulation, where $r^2$ values are found to be 0.838 and 0.708 for 2x$CO_2$ and 4x$CO_2$, respectively. A correlation is also seen in the *RAD* simulation at 2x$CO_2$ ($r^2$ value of 0.601), however the correlation in the *RAD* simulation does not hold at 4x$CO_2$, where the $r^2$ value reduces to 0.265. The reduced correlation in the *RAD* simulation at 4x$CO_2$ suggests

a reduced relationship between NPP and $\tau_s$ at the more extreme temperature changes that are projected at high levels of
300 atmospheric $CO_2$ (without the direct effects of $CO_2$ in this run).

For each CMIP6 ESM, NPP and $\tau_s$ are found to be strongly inversely correlated in the *full* 1% $CO_2$ simulation (Fig. 9). The
$r^2$ values between $NPP/NPP_0$ and $\tau_{s,0}/\tau_s$ (where the subscript 0 denotes the historical state) are found to be greater than 0.95
in all models except for ACCESS-ESM1-5 (where an $r^2$ value of 0.65 is found due to a breakdown at high $CO_2$ levels). In the
*BGC* simulation, a similar relationship between $NPP/NPP_0$ and $\tau_{s,0}/\tau_s$ is seen up until approximately 2x$CO_2$ in all ESMs
305 (approximately 50% of the simulation). However, how the relationship between $NPP/NPP_0$ and $\tau_{s,0}/\tau_s$ changes throughout
the *BGC* simulation (between 2x$CO_2$ and 4x$CO_2$) varies between models. A greater rate of $NPP/NPP_0$ increase compared
to $\tau_{s,0}/\tau_s$ is seen at greater levels of climate forcing for the majority of CMIP6 ESMs (BCC-CSM2-MR, CanESM5, GFDL-
ESM4, IPSL-CM6A-LR, MIROC-ES2L, MPI-ESM1-2-LR and UKESM1-0-LL), where the $\tau_s$ changes appear to saturate and
a limit to the increase is seen. In these ESMs, the changes seen in the *full* and *BGC* simulations differ due to a climate effect
310 (shown by the *RAD* simulation), which appears to negate the apparent limit or saturation seen in the $\tau_{s,0}/\tau_s$ increase in the
*BGC* simulation (Fig. 9). In CESM2 and NorESM2-LM (containing the same land surface model component), a consistent
relationship is seen in both the *full* 1% $CO_2$ and *BGC* simulations, suggesting the changes in NPP and $\tau_s$ are primarily driven
by changes in $CO_2$ concentrations or that the climate affects cancel out to a resultant net zero change. In ACCESS-ESM1-5,
a consistent relationship is seen in the *full* 1% $CO_2$, *BGC* and *RAD* simulations, suggesting a greater sensitivity of NPP to
315 environmental climate changes compared to the other CMIP6 ESMs (Fig. 9).

It has been shown in this subsection that the correlation between $\Delta C_{s,NPP}$ and $\Delta C_{s,\tau}$, as seen in the SSP simulations (Fig.
7 and Fig. 8), is also evident in the *full* 1% $CO_2$ C4MIP simulation. This suggests the relationship is not a result of additional
processes included in the SSP simulations compared to the C4MIP experiments, such as land use change (Jones et al., 2016). An
additional explanation for the coupling could be similarities in the modelled sensitivities of NPP and $R_h$ to changes in climate
320 (i.e. temperature and moisture changes). For example, if NPP and soil respiration rate both increased with warming, a negative
correlation between $\Delta C_{s,NPP}$ and $\Delta C_{s,\tau}$ would be seen. However, under these circumstances the negative correlation would
not be seen in the $CO_2$ only runs (*BGC* simulation), as there is no global warming in these simulations (see Methods). Instead,
a reduction in effective soil carbon turnover time is seen in the $CO_2$ only runs (*BGC* simulation; Fig. A2), which implies a
non-climate response in $\tau_s$ and results in a NPP-$\tau_s$ negative correlation under changing atmospheric $CO_2$ alone (Fig. 9). Fig.
325 10 shows that the change in the effective soil carbon turnover time in the $CO_2$ only simulation (*BGC* simulation) accounts for
at least 50% of the total change in the effective soil carbon turnover time in the *full* 1% simulation across CMIP6 ESMs.

### 3.5 The role of false priming

Koven et al. (2015) presents the concept of false priming as a reduction in effective soil carbon turnover time ($\tau_s$) due to
increases in productivity (NPP). It was defined as 'false priming' due to the impact being similar to the 'true priming' process,
330 but occurs without simulating the priming mechanisms; where priming is defined as the stimulation of decomposition of soil
carbon (reducing $\tau_s$) due to input of carbon to the soil (Liu et al., 2020). The false priming reduction in effective $\tau_s$ is a transient
phenomenon that arises in soil models that represent multiple carbon pools with different turnover times. Under continually

increasing NPP, proportionally more of the additional input litter carbon is put into the faster soil carbon pools than the slow, which brings down the global average effective $\tau_s$ value of the soil. In this subsection, false priming is explored as a possible
335 explanation for the negative correlation seen between NPP and $\tau_s$, which are seen even in the *BGC* simulations ($CO_2$ only) where the climate does not change significantly (Fig. 10).

Koven et al. (2015) demonstrates false priming with a simple three-box soil carbon model, which has been adapted here to use notation consistent with the rest of this study:

$$\frac{dC_{s,1}}{dt} = NPP - \frac{C_{s,1}}{\tau_{s,1}} \tag{13}$$

340
$$\frac{dC_{s,2}}{dt} = \frac{e_1 C_{s,1}}{\tau_{s,1}} - \frac{C_{s,2}}{\tau_{s,2}} \tag{14}$$

$$\frac{dC_{s,3}}{dt} = \frac{e_2 C_{s,2}}{\tau_{s,2}} - \frac{C_{s,3}}{\tau_{s,3}} \tag{15}$$

$$R_h = \frac{(1-e_1)C_{s,1}}{\tau_{s,1}} + \frac{(1-e_2)C_{s,2}}{\tau_{s,2}} + \frac{(1-e_3)C_{s,3}}{\tau_{s,3}} \tag{16}$$

$$C_s = C_{s,1} + C_{s,2} + C_{s,3} \tag{17}$$

$$\tau_{s,1} = 1, \tau_{s,2} = 10, \tau_{s,3} = 100, e_1 = 0.3, e_2 = 0.3, e_3 = 0. \tag{18}$$

345 where, $C_{s,1}$, $C_{s,2}$, $C_{s,3}$ represent the carbon stored in soil carbon pools 1, 2, and 3 and make up the total soil carbon ($C_s$). Similarly, $\tau_{s,i}$ are the respective soil carbon turnover times, which are given defined values of increasing turnover times in years: fast (1 year), medium (10 years) and slow (100 years). NPP represents the carbon input into the system, where carbon is inputted into pool 1 ($C_{s,1}$), then flows to pool 2 ($C_{s,2}$) and then 3 ($C_{s,3}$). The coefficients $e_i$ represents the fraction of carbon that is passed to the next pool rather than outputted as heterotrophic respiration ($R_h$).

350 At equilibrium, the change in the soil carbon pools will be zero ($dC_{s,i}/dt = 0$), so the amount of soil carbon present within each pool depends on the input carbon and turnover time of the pool ($\tau_{s,i}$). Under increasing NPP, the three-box model can be used to investigate the subsequent changes to soil carbon in the 3 carbon pools ($C_{s,1}$, $C_{s,2}$, $C_{s,3}$) based on changing input alone, due to each pool having a fixed $\tau_{s,i}$ value. This removes the $\Delta\tau_s$ from changing environmental and microbial conditions (Koven et al., 2015; Wieder et al., 2015a; Exbrayat et al., 2013). The effective $\tau_s$ of the system is calculated by definition (using
355 Equation 1).

Fig. 11(a) shows a simulation of the response of this three-box model to an NPP input flux that increases at 0.3% per year, and where the soil carbon boxes are initialised at 0 (reproducing Fig. 12 in Koven et al. (2015)). The greater fraction of $\Delta C_s$ in the fast soil carbon pool compared to the slow can be seen, which results in a decline in the effective $\tau_s$ of the system. This

decline in effective $\tau_s$ with increasing NPP is clear and demonstrates false priming (Fig. 11(a)). Fig. 11(b) again demonstrates that false priming is a transient effect associated with the distribution of soil carbon between the 3 pools, which emerges from the differences in the mass-weighted and flux-weighted responses. It shows results from the same model, but for a step increase in global NPP from 50 PgC yr$^{-1}$ to 70 PgC yr$^{-1}$ at year 100. The fast soil carbon pool reaches equilibrium before the slower soil carbon pool resulting in the instantaneous decline in $\tau_s$ of about 10%, which eventually reduces to return the soil to the original $\tau_s$. This transient effect occurs on the timescale of the slowest carbon pool, and therefore may take many centuries.

The same three-box model can also be used to investigate the relationship between the contributions of changes in NPP ($\Delta C_{s,NPP}$) and $\tau_s$ ($\Delta C_{s,\tau}$) to net soil carbon change that was noted in both Fig. 7 and Fig. 8. Fig. 12 plots $\Delta C_{s,NPP}$ against $\Delta C_{s,\tau}$ from the three-box model after 70 years of runs that assume different rates of increase of NPP (0% to 0.8% per year in increments of 0.05%). A clear relationship between $\Delta C_{s,NPP}$ and $\Delta C_{s,\tau}$ is seen, with greater false priming (more negative $\Delta C_{s,\tau}$) when the NPP increase is larger (more positive $\Delta C_{s,NPP}$). The similarity of Fig. 12 to both Fig. 7 and Fig. 8 is clear, suggesting that false priming and the structure of the soil carbon models within the ESMs is likely contributing to these correlations in CMIP6 (and to a lesser extent in CMIP5).

It is noted that the influence of false priming was stronger in the *full* 1% $CO_2$ and *BGC* ($CO_2$ only) simulations, compared to the *RAD* (climate only) simulation (Fig. 8). This is likely due to the *RAD* simulation not seeing sufficient NPP change, and therefore sufficient input of soil carbon, for the false priming effect to be significant (see Fig. A2). Additionally, the direct effect of temperature changes on $\tau_s$ in the *RAD* simulation (in the absence of atmospheric $CO_2$ changes) is likely to dampen the correlation to NPP changes, due to both direct and indirect $\Delta \tau_s$ influences in this case (Varney et al., 2020).

False priming refers to a reduction in the effective turnover time when the input of carbon into the soil increases. It was named 'false priming' as it can look like the increase in heterotrophic respiration that occurs when a soil microbial community is stimulated by the addition of labile carbon or nutrients ('true priming'). However, 'false priming' is arguably a misleading term because it is a real effect. It arises as a result of a change in the relative quantities of carbon turning over at different rates, which occurs transiently in response to an increase in the input of carbon into the soil. In the context of our three-box model, for example, the turnover rates of each individual box do not change. However, because each box responds differently to the increase in NPP, a difference in the average or effective turnover (i.e. as defined in Equation 1) is seen. The effective soil carbon turnover time is a measure of how long carbon remains in the soil. However, it cannot necessarily be assumed that all carbon will take exactly the same amount of time to be re-released. Different types of litter input (e.g. lignin vs carbohydrate) take different amounts of time to decompose (Krishna and Mohan, 2017). Similarly, vertical gradients in temperature throughout the soil result in variations of turnover time within the system (Koven et al., 2017). The effective carbon turnover time is an average of these distributions of turnover times and an increase in the amount of fast turnover carbon in the system relative to slower turnover carbon results in it decreasing. As it has been shown here, this effect can be significant and must be accounted for when attributing soil carbon change to different environmental drivers (Georgiou et al., 2015).

This study has highlighted how false priming has contributed to a reduced spread in $\Delta C_s$ ESM projections in CMIP6, due to a cancellation effect seen between increases due to $\Delta$NPP ($\Delta C_{s,NPP}$) and decreases due to $\Delta \tau_s$ ($\Delta C_{s,\tau}$). The extent of false priming within ESM projections will depend on the distribution of carbon within soil carbon pools and how litter carbon

is allocated between pools with fast and slow turnover times (Koven et al., 2015). Fig. 10(c) shows the fraction of $\Delta\tau_s$ due to $\Delta CO_2$, which can be used as a proxy to estimate the contribution of false priming to the overall projected $\Delta\tau_s$ in CMIP6 ESMs, which varies between approximately 50% (CanESM5 and MIROC-ES2L) to 90% (CESM2 and NorESM2-LM). A more apparent false priming affect within CMIP6 could suggest an improved representation of the slower components of soil carbon since CMIP5, commonly by including more dead carbon pools within the ESM (Table 1). Based on observational radiocarbon estimates it has been found that CMIP5 ESMs underestimate carbon age within the soil (He et al., 2016; Shi et al., 2020), suggesting that ESMs underestimate the amount of carbon in the slow carbon pools. It has been shown that representing soil carbon ages more in line with radiocarbon estimates leads to a reduced potential for soil carbon sequestration in the future (He et al., 2016), which agrees qualitatively with the projected 21$^{st}$ century soil carbon changes as predicted by CMIP6 compared to CMIP5 found in this study.

On top of the role of false priming, additional factors influence the magnitude of predicted $\Delta C_s$ within ESMs. Generationally related ESMs between CMIP5 and CMIP6 allow us to highlight some key changes between the CMIP generations and to suggest potential model developments which may have contributed to the projected differences in future $C_s$ seen here. For example, within CMIP5 the models HadGEM2-ES and MPI-ESM-LR predicted the greatest increases in soil carbon within the ensemble, however within CMIP6 the updated versions UKESM1-0-LL and MPI-ESM1-2-LR predict reduced increases (Fig. 1). Both updated variants of these ESMs include the representation of interactive nitrogen in CMIP6 simulations (Table 1), which could limit carbon sequestration through limiting the magnitude of $CO_2$ fertilisation. Depending on the ratio of carbon to nitrogen within the soil however, accelerated decomposition due to soil warming can increase nitrogen mineralisation and alleviate the nutrient limitation in plants (Wiltshire et al., 2021). Additionally, MPI-ESM1-2-LR (CMIP6) sees an increased number of dead or soil carbon pools compared with MPI-ESM-LR (CMIP5), whereas UKESM1-0-LL (CMIP6) from HadGEM2-ES (CMIP5) sees no change in the number of carbon pools. The increased number of dead carbon pools could contribute to the decrease in $\Delta C_s$ by either: a transient reduction due to false priming, or longer soil carbon turnover times resulting in carbon being stored in slower pools within the soil. It is noted that an investigation into the role of soil carbon pools in future soil carbon projections will require data for projections and allocation of $C_s$ in individual soil pools within ESMs, which is beyond the scope of this study (Koven et al., 2015).

## 4    Conclusions

In this study, future projections of soil carbon change ($\Delta C_s$) have been analysed using ESM output from the latest CMIP6 ensemble and were investigated under differing levels of climate change (future scenarios *SSP126*, *SSP245* and *SSP585*). The future projections made by CMIP6 ESMs were also compared against equivalent projections made by the previous generation of ESMs in the CMIP5 ensemble (future scenarios *RCP2.6*, *RCP4.5* and *RCP8.5*) to investigate whether recent model improvements have reduced the uncertainty surrounding the future soil carbon response. Additionally, $\Delta C_s$ was broken down into the individual components which contribute to the net change within ESMs, with a specific focus on increases due to increases in NPP ($\Delta C_{s,NPP}$) and decreases due to reductions in turnover ($\Delta C_{s,\tau}$). Below the key conclusions from this study are listed.

1. An apparent reduction in uncertainty of end of 21$^{st}$ century $\Delta C_s$ projections is suggested in CMIP6 compared to CMIP5.

2. However, the same reduction in projection uncertainty is not suggested surrounding the soil carbon controls: Net Primary Productivity (NPP) and the effective soil carbon turnover time ($\tau_s = C_s/R_h$), and the subsequent effects on future soil carbon storage ($\Delta C_{s,NPP}$ and $\Delta C_{s,\tau}$, respectively).

3. The derived linear terms which contribute to net soil carbon change, the response of soil carbon due to changes in NPP ($\Delta C_{s,NPP}$) and the response due to changes in $\tau_s$ ($\Delta C_{s,\tau}$), are found to have a strong relationship in CMIP6, with a more significant correlation than what was seen in CMIP5. This correlation is likely to be a cause of the reduction in the $\Delta C_s$ projection spread across the CMIP6 ensemble.

4. False priming was found to likely be contributing to the apparent emergent relationship between $\Delta C_{s,NPP}$ and $\Delta C_{s,\tau}$ in CMIP6 ESMs, which describes a transient reduction in effective soil carbon turnover time due to increased input of carbon to the soil. The net effect of false priming is a coupling affect between $\Delta NPP$ and $\Delta \tau_s$ and results in a reduced range of future $\Delta C_s$ predictions in CMIP6.

5. Our study highlights the significant role that false priming can play under transient changes in atmospheric $CO_2$ and climate. We advise caution in the interpretation of changes in the effective soil carbon turnover time in terms of climate affects alone. Idealised C4MIP simulations, which can be used to separate the effects of $CO_2$ and climate on the effective soil carbon turnover time, are very useful to assess the role of false priming in models. Understanding these factors will be key to predicting soil carbon changes over the next 100 years.

Understanding and quantifying soil carbon feedbacks under anthropogenic emissions of $CO_2$ is critical for calculating an accurate global carbon budget, which is required if Paris Agreement targets are to be met (Friedlingstein et al., 2022). This study highlights the importance of considering the individual soil driven carbon feedbacks under climate change when determining the overall response of global soil carbon storage, and suggests the need for constraints on the magnitudes of these feedbacks in CMIP6 to reduce uncertainty in projections of future land carbon storage.

*Code availability.* Code is available on GitHub (https://github.com/rebeccamayvarney/CMIP6_dCs).

*Data availability.* The CMIP data analysed during this study are available online: CMIP6 (https://esgf-node.llnl.gov/search/cmip6/) and CMIP5 (https://esgf-node.llnl.gov/search/cmip5/).

*Author contributions.* RMV, SEC and PMC outlined the study. RMV completed the analysis and produced the figures. All the co-authors provided guidance on the study at various times and suggested edits to the draft manuscript.

*Competing interests.* The authors have declared no competing interests.

455 *Acknowledgements.* This research has been supported by the European Research Council, Emergent Constraints on Climate–Land feedbacks in the Earth System project (ECCLES; grant no. 742472) and Climate–Carbon Interactions in the Current Century project (4C; grant no. 821003) (RMV and PMC). SEC was supported by a Natural Environment Research Council independent research fellowship (grant no. NE/R015791/1). AJW and EJB were supported by the Joint UK BEIS/Defra Met Office Hadley Centre Climate Programme (grant no. GA01101). SJ was supported by the Brazilian ecosystem resilience in net-generation vegetation dynamics scheme (CSSP Brazil; project
460 P109647). We thank the World Climate Research Programme's Working Group on Coupled Modelling and the climate modelling groups for producing and making their model output available.

# References

Arora, V. and Boer, G.: Uncertainties in the 20th century carbon budget associated with land use change, Global Change Biology, 16, 3327–3348, 2010.

465 Arora, V., Boer, G., Christian, J., Curry, C., Denman, K., Zahariev, K., Flato, G., Scinocca, J., Merryfield, W., and Lee, W.: The effect of terrestrial photosynthesis down regulation on the twentieth-century carbon budget simulated with the CCCma Earth System Model, Journal of Climate, 22, 6066–6088, 2009.

Arora, V. K., Boer, G. J., Friedlingstein, P., Eby, M., Jones, C. D., Christian, J. R., Bonan, G., Bopp, L., Brovkin, V., Cadule, P., et al.: Carbon–concentration and carbon–climate feedbacks in CMIP5 Earth system models, Journal of Climate, 26, 5289–5314, 2013.

470 Arora, V. K., Katavouta, A., Williams, R. G., Jones, C. D., Brovkin, V., Friedlingstein, P., Schwinger, J., Bopp, L., Boucher, O., Cadule, P., et al.: Carbon–concentration and carbon–climate feedbacks in CMIP6 models and their comparison to CMIP5 models, Biogeosciences, 17, 4173–4222, 2020.

Bentsen, M., Bethke, I., Debernard, J. B., Iversen, T., Kirkevåg, A., Seland, Ø., Drange, H., Roelandt, C., Seierstad, I. A., Hoose, C., et al.: The Norwegian Earth System Model, NorESM1-M–Part 1: description and basic evaluation of the physical climate, Geoscientific Model

475 Development, 6, 687–720, 2013.

Best, M., Pryor, M., Clark, D., Rooney, G., Essery, R., Ménard, C., Edwards, J., Hendry, M., Porson, A., Gedney, N., et al.: The Joint UK Land Environment Simulator (JULES), model description–Part 1: energy and water fluxes, Geoscientific Model Development, 4, 677–699, 2011.

Boucher, O., Servonnat, J., Albright, A. L., Aumont, O., Balkanski, Y., Bastrikov, V., Bekki, S., Bonnet, R., Bony, S., Bopp, L., et al.:

480 Presentation and evaluation of the IPSL-CM6A-LR climate model, Journal of Advances in Modeling Earth Systems, 12, e2019MS002 010, 2020.

Burke, E. J., Ekici, A., Huang, Y., Chadburn, S. E., Huntingford, C., Ciais, P., Friedlingstein, P., Peng, S., and Krinner, G.: Quantifying uncertainties of permafrost carbon–climate feedbacks, Biogeosciences, 14, 3051–3066, 2017.

Burke, E. J., Zhang, Y., and Krinner, G.: Evaluating permafrost physics in the Coupled Model Intercomparison Project 6 (CMIP6) models

485 and their sensitivity to climate change, The Cryosphere, 14, 3155–3174, 2020.

Canadell, J., Monteiro, P., Costa, M., Cotrim da Cunha, L., Cox, P., Eliseev, A., Henson, S., Ishii, M., Jaccard, S., Koven, C., Lohila, A., Patra, P., Piao, S., Rogelj, J., Syampungani, S., Zaehle, S., and Zickfeld, K.: Global Carbon and other Biogeochemical Cycles and Feedbacks, Cambridge University Press, Cambridge, United Kingdom and New York, NY, USA, https://doi.org/10.1017/9781009157896.007, 2021.

Cheruy, F., Ducharne, A., Hourdin, F., Musat, I., Vignon, É., Gastineau, G., Bastrikov, V., Vuichard, N., Diallo, B., Dufresne, J.-L., et al.:

490 Improved near-surface continental climate in IPSL-CM6A-LR by combined evolutions of atmospheric and land surface physics, Journal of Advances in Modeling Earth Systems, 12, e2019MS002 005, 2020.

Clark, D., Mercado, L., Sitch, S., Jones, C., Gedney, N., Best, M., Pryor, M., Rooney, G., Essery, R., Blyth, E., et al.: The Joint UK Land Environment Simulator (JULES), model description–Part 2: carbon fluxes and vegetation dynamics, Geoscientific Model Development, 4, 701–722, 2011.

495 Cox, P. M., Betts, R. A., Jones, C. D., Spall, S. A., and Totterdell, I. J.: Acceleration of global warming due to carbon-cycle feedbacks in a coupled climate model, Nature, 408, 184, 2000.

Crowther, T. W., Todd-Brown, K. E., Rowe, C. W., Wieder, W. R., Carey, J. C., Machmuller, M. B., Snoek, B., Fang, S., Zhou, G., Allison, S. D., et al.: Quantifying global soil carbon losses in response to warming, Nature, 540, 104, 2016.

Dai, Y., Zeng, X., Dickinson, R. E., Baker, I., Bonan, G. B., Bosilovich, M. G., Denning, A. S., Dirmeyer, P. A., Houser, P. R., Niu, G., et al.: The common land model, Bulletin of the American Meteorological Society, 84, 1013–1024, 2003.

Danabasoglu, G., Lamarque, J.-F., Bacmeister, J., Bailey, D., DuVivier, A., Edwards, J., Emmons, L., Fasullo, J., Garcia, R., Gettelman, A., et al.: The community earth system model version 2 (CESM2), Journal of Advances in Modeling Earth Systems, 12, 2020.

Davies-Barnard, T., Meyerholt, J., Zaehle, S., Friedlingstein, P., Brovkin, V., Fan, Y., Fisher, R. A., Jones, C. D., Lee, H., Peano, D., et al.: Nitrogen cycling in CMIP6 land surface models: progress and limitations, Biogeosciences, 17, 5129–5148, 2020.

Delire, C., Séférian, R., Decharme, B., Alkama, R., Calvet, J.-C., Carrer, D., Gibelin, A.-L., Joetzjer, E., Morel, X., Rocher, M., et al.: The global land carbon cycle simulated with ISBA-CTRIP: Improvements over the last decade, Journal of Advances in Modeling Earth Systems, 12, e2019MS001 886, 2020.

Dufresne, J.-L., Foujols, M.-A., Denvil, S., Caubel, A., Marti, O., Aumont, O., Balkanski, Y., Bekki, S., Bellenger, H., Benshila, R., et al.: Climate change projections using the IPSL-CM5 Earth System Model: from CMIP3 to CMIP5, Climate dynamics, 40, 2123–2165, 2013.

Dunne, J., Horowitz, L., Adcroft, A., Ginoux, P., Held, I., John, J., Krasting, J., Malyshev, S., Naik, V., Paulot, F., et al.: The GFDL Earth System Model version 4.1 (GFDL-ESM 4.1): Overall coupled model description and simulation characteristics, Journal of Advances in Modeling Earth Systems, 12, e2019MS002 015, 2020.

Dunne, J. P., John, J. G., Adcroft, A. J., Griffies, S. M., Hallberg, R. W., Shevliakova, E., Stouffer, R. J., Cooke, W., Dunne, K. A., Harrison, M. J., et al.: GFDL's ESM2 global coupled climate–carbon earth system models. Part I: Physical formulation and baseline simulation characteristics, Journal of climate, 25, 6646–6665, 2012.

Dunne, J. P., John, J. G., Shevliakova, E., Stouffer, R. J., Krasting, J. P., Malyshev, S. L., Milly, P., Sentman, L. T., Adcroft, A. J., Cooke, W., et al.: GFDL's ESM2 global coupled climate–carbon earth system models. Part II: carbon system formulation and baseline simulation characteristics, Journal of Climate, 26, 2247–2267, 2013.

Exbrayat, J.-F., Pitman, A., Zhang, Q., Abramowitz, G., and Wang, Y.-P.: Examining soil carbon uncertainty in a global model: response of microbial decomposition to temperature, moisture and nutrient limitation, Biogeosciences, 10, 7095–7108, 2013.

Eyring, V., Bony, S., Meehl, G. A., Senior, C. A., Stevens, B., Stouffer, R. J., and Taylor, K. E.: Overview of the Coupled Model Intercomparison Project Phase 6 (CMIP6) experimental design and organization, Geoscientific Model Development (Online), 9, 2016.

Friedlingstein, P., Cox, P., Betts, R., Bopp, L., von Bloh, W., Brovkin, V., Cadule, P., Doney, S., Eby, M., Fung, I., et al.: Climate–carbon cycle feedback analysis: results from the C4MIP model intercomparison, Journal of climate, 19, 3337–3353, 2006.

Friedlingstein, P., O'sullivan, M., Jones, M. W., Andrew, R. M., Gregor, L., Hauck, J., Le Quéré, C., Luijkx, I. T., Olsen, A., Peters, G. P., et al.: Global carbon budget 2022, Earth System Science Data, 14, 4811–4900, 2022.

Georgiou, K., Koven, C. D., Riley, W. J., and Torn, M. S.: Toward improved model structures for analyzing priming: potential pitfalls of using bulk turnover time, Global Change Biology, 21, 4298–4302, 2015.

Goll, D. S., Brovkin, V., Liski, J., Raddatz, T., Thum, T., and Todd-Brown, K. E.: Strong dependence of CO2 emissions from anthropogenic land cover change on initial land cover and soil carbon parametrization, Global Biogeochemical Cycles, 29, 1511–1523, 2015.

Goll, D. S., Winkler, A. J., Raddatz, T., Dong, N., Prentice, I. C., Ciais, P., and Brovkin, V.: Carbon–nitrogen interactions in idealized simulations with JSBACH (version 3.10), Geoscientific Model Development, 10, 2009–2030, 2017.

Green, J. K., Seneviratne, S. I., Berg, A. M., Findell, K. L., Hagemann, S., Lawrence, D. M., and Gentine, P.: Large influence of soil moisture on long-term terrestrial carbon uptake, Nature, 565, 476–479, 2019.

Guimberteau, M., Zhu, D., Maignan, F., Huang, Y., Yue, C., Dantec-Nédélec, S., Ottlé, C., Jornet-Puig, A., Bastos, A., Laurent, P., et al.: ORCHIDEE-MICT (v8. 4.1), a land surface model for the high latitudes: model description and validation, Geoscientific Model Development, 11, 121–163, 2018.

Hajima, T., Watanabe, M., Yamamoto, A., Tatebe, H., Noguchi, M. A., Abe, M., Ohgaito, R., Ito, A., Yamazaki, D., Okajima, H., et al.: Development of the MIROC-ES2L Earth system model and the evaluation of biogeochemical processes and feedbacks, Geoscientific Model Development, 13, 2197–2244, 2020.

Haverd, V., Smith, B., Nieradzik, L., Briggs, P. R., Woodgate, W., Trudinger, C. M., Canadell, J. G., and Cuntz, M.: A new version of the CABLE land surface model (Subversion revision r4601) incorporating land use and land cover change, woody vegetation demography, and a novel optimisation-based approach to plant coordination of photosynthesis, Geoscientific Model Development, 11, 2995–3026, 2018.

He, Y., Trumbore, S. E., Torn, M. S., Harden, J. W., Vaughn, L. J., Allison, S. D., and Randerson, J. T.: Radiocarbon constraints imply reduced carbon uptake by soils during the 21st century, Science, 353, 1419–1424, 2016.

Hugelius, G., Loisel, J., Chadburn, S., Jackson, R. B., Jones, M., MacDonald, G., Marushchak, M., Olefeldt, D., Packalen, M., Siewert, M. B., et al.: Large stocks of peatland carbon and nitrogen are vulnerable to permafrost thaw, Proceedings of the National Academy of Sciences, 117, 20 438–20 446, 2020.

Ito, A. and Oikawa, T.: A simulation model of the carbon cycle in land ecosystems (Sim-CYCLE): a description based on dry-matter production theory and plot-scale validation, Ecological modelling, 151, 143–176, 2002.

Iversen, T., Bentsen, M., Bethke, I., Debernard, J., Kirkevåg, A., Seland, Ø., Drange, H., Kristjansson, J., Medhaug, I., Sand, M., et al.: The Norwegian earth system model, NorESM1-M–Part 2: climate response and scenario projections, Geoscientific Model Development, 6, 389–415, 2013.

Jackson, R. B., Lajtha, K., Crow, S. E., Hugelius, G., Kramer, M. G., and Piñeiro, G.: The ecology of soil carbon: pools, vulnerabilities, and biotic and abiotic controls, Annual Review of Ecology, Evolution, and Systematics, 48, 419–445, 2017.

Jenkinson, D., Adams, D., and Wild, A.: Model estimates of CO2 emissions from soil in response to global warming, Nature, 351, 304–306, 1991.

Ji, D., Wang, L., Feng, J., Wu, Q., Cheng, H., Zhang, Q., Yang, J., Dong, W., Dai, Y., Gong, D., et al.: Description and basic evaluation of Beijing Normal University Earth system model (BNU-ESM) version 1, Geoscientific Model Development, 7, 2039–2064, 2014.

Ji, J., Huang, M., and Li, K.: Prediction of carbon exchanges between China terrestrial ecosystem and atmosphere in 21st century, Science in China Series D: Earth Sciences, 51, 885–898, 2008.

Jones, C., Hughes, J., Bellouin, N., Hardiman, S., Jones, G., Knight, J., Liddicoat, S., O'connor, F., Andres, R. J., Bell, C., et al.: The HadGEM2-ES implementation of CMIP5 centennial simulations, Geoscientific Model Development, 4, 543–570, 2011.

Jones, C. D., Arora, V., Friedlingstein, P., Bopp, L., Brovkin, V., Dunne, J., Graven, H., Hoffman, F., Ilyina, T., John, J. G., et al.: C4MIP–The coupled climate–carbon cycle model intercomparison project: Experimental protocol for CMIP6, Geoscientific Model Development, 9, 2853–2880, 2016.

Knorr, W.: Annual and interannual CO2 exchanges of the terrestrial biosphere: Process-based simulations and uncertainties, Global Ecology and Biogeography, 9, 225–252, 2000.

Koven, C. D., Chambers, J. Q., Georgiou, K., Knox, R., Negron-Juarez, R., Riley, W. J., Arora, V. K., Brovkin, V., Friedlingstein, P., and Jones, C. D.: Controls on terrestrial carbon feedbacks by productivity versus turnover in the CMIP5 Earth System Models, Biogeosciences, 12, 5211–5228, https://doi.org/10.5194/bg-12-5211-2015, 2015.

Koven, C. D., Hugelius, G., Lawrence, D. M., and Wieder, W. R.: Higher climatological temperature sensitivity of soil carbon in cold than warm climates, Nature Climate Change, 7, 817–822, 2017.

Krinner, G., Viovy, N., de Noblet-Ducoudré, N., Ogée, J., Polcher, J., Friedlingstein, P., Ciais, P., Sitch, S., and Prentice, I. C.: A dynamic 575 global vegetation model for studies of the coupled atmosphere-biosphere system, Global Biogeochemical Cycles, 19, 2005.

Krishna, M. and Mohan, M.: Litter decomposition in forest ecosystems: a review, Energy, Ecology and Environment, 2, 236–249, 2017.

Lawrence, D. M., Oleson, K. W., Flanner, M. G., Thornton, P. E., Swenson, S. C., Lawrence, P. J., Zeng, X., Yang, Z.-L., Levis, S., Sakaguchi, K., et al.: Parameterization improvements and functional and structural advances in version 4 of the Community Land Model, Journal of Advances in Modeling Earth Systems, 3, 2011.

580 Lawrence, D. M., Fisher, R. A., Koven, C. D., Oleson, K. W., Swenson, S. C., Bonan, G., Collier, N., Ghimire, B., Van Kampenhout, L., Kennedy, D., et al.: The Community Land Model version 5: Description of new features, benchmarking, and impact of forcing uncertainty, Journal of Advances in Modeling Earth Systems, 11, 4245–4287, 2019.

Liu, X.-J. A., Finley, B. K., Mau, R. L., Schwartz, E., Dijkstra, P., Bowker, M. A., and Hungate, B. A.: The soil priming effect: Consistent across ecosystems, elusive mechanisms, Soil Biology and Biochemistry, 140, 107 617, 2020.

585 Mauritsen, T., Bader, J., Becker, T., Behrens, J., Bittner, M., Brokopf, R., Brovkin, V., Claussen, M., Crueger, T., Esch, M., et al.: Developments in the MPI-M Earth System Model version 1.2 (MPI-ESM1. 2) and its response to increasing CO2, Journal of Advances in Modeling Earth Systems, 11, 998–1038, 2019.

Meinshausen, M., Smith, S. J., Calvin, K., Daniel, J. S., Kainuma, M., Lamarque, J.-F., Matsumoto, K., Montzka, S., Raper, S., Riahi, K., et al.: The RCP greenhouse gas concentrations and their extensions from 1765 to 2300, Climatic change, 109, 213, 2011.

590 Melton, J. R., Arora, V. K., Wisernig-Cojoc, E., Seiler, C., Fortier, M., Chan, E., and Teckentrup, L.: CLASSIC v1. 0: the open-source community successor to the Canadian Land Surface Scheme (CLASS) and the Canadian Terrestrial Ecosystem Model (CTEM)–Part 1: Model framework and site-level performance, Geoscientific Model Development, 13, 2825–2850, 2020.

O'Neill, B. C., Tebaldi, C., Vuuren, D. P. v., Eyring, V., Friedlingstein, P., Hurtt, G., Knutti, R., Kriegler, E., Lamarque, J.-F., Lowe, J., et al.: The scenario model intercomparison project (ScenarioMIP) for CMIP6, Geoscientific Model Development, 9, 3461–3482, 2016.

595 O'Neill, B. C., Kriegler, E., Riahi, K., Ebi, K. L., Hallegatte, S., Carter, T. R., Mathur, R., and van Vuuren, D. P.: A new scenario framework for climate change research: the concept of shared socioeconomic pathways, Climatic change, 122, 387–400, 2014.

Parton, W. J., Stewart, J. W., and Cole, C. V.: Dynamics of C, N, P and S in grassland soils: a model, Biogeochemistry, 5, 109–131, 1988.

Raddatz, T., Reick, C., Knorr, W., Kattge, J., Roeckner, E., Schnur, R., Schnitzler, K.-G., Wetzel, P., and Jungclaus, J.: Will the tropical land biosphere dominate the climate–carbon cycle feedback during the twenty-first century?, Climate dynamics, 29, 565–574, 2007.

600 Sato, H., Itoh, A., and Kohyama, T.: SEIB–DGVM: A new Dynamic Global Vegetation Model using a spatially explicit individual-based approach, Ecological Modelling, 200, 279–307, 2007.

Schimel, D., Stephens, B. B., and Fisher, J. B.: Effect of increasing CO2 on the terrestrial carbon cycle, Proceedings of the National Academy of Sciences, 112, 436–441, 2015.

Schmidt, G. A., Kelley, M., Nazarenko, L., Ruedy, R., Russell, G. L., Aleinov, I., Bauer, M., Bauer, S. E., Bhat, M. K., Bleck, R., et al.: 605 Configuration and assessment of the GISS ModelE2 contributions to the CMIP5 archive, Journal of Advances in Modeling Earth Systems, 6, 141–184, 2014.

Schmidt, M. W., Torn, M. S., Abiven, S., Dittmar, T., Guggenberger, G., Janssens, I. A., Kleber, M., Kögel-Knabner, I., Lehmann, J., Manning, D. A., et al.: Persistence of soil organic matter as an ecosystem property, Nature, 478, 49–56, 2011.

Schuur, E. A., Abbott, B. W., Commane, R., Ernakovich, J., Euskirchen, E., Hugelius, G., Grosse, G., Jones, M., Koven, C., Leshyk, V., et al.: Permafrost and climate change: carbon cycle feedbacks from the warming Arctic, Annual Review of Environment and Resources, 47, 343–371, 2022.

Séférian, R., Nabat, P., Michou, M., Saint-Martin, D., Voldoire, A., Colin, J., Decharme, B., Delire, C., Berthet, S., Chevallier, M., et al.: Evaluation of CNRM earth system model, CNRM-ESM2-1: Role of earth system processes in present-day and future climate, Journal of Advances in Modeling Earth Systems, 11, 4182–4227, 2019.

Seiler, C., Melton, J. R., Arora, V. K., and Wang, L.: CLASSIC v1. 0: the open-source community successor to the Canadian Land Surface Scheme (CLASS) and the Canadian Terrestrial Ecosystem Model (CTEM)–Part 2: Global benchmarking, Geoscientific Model Development, 14, 2371–2417, 2021.

Seland, Ø., Bentsen, M., Olivié, D., Toniazzo, T., Gjermundsen, A., Graff, L. S., Debernard, J. B., Gupta, A. K., He, Y.-C., Kirkevåg, A., et al.: Overview of the Norwegian Earth System Model (NorESM2) and key climate response of CMIP6 DECK, historical, and scenario simulations, Geoscientific Model Development, 13, 6165–6200, 2020.

Sellar, A. A., Walton, J., Jones, C. G., Wood, R., Abraham, N. L., Andrejczuk, M., Andrews, M. B., Andrews, T., Archibald, A. T., de Mora, L., et al.: Implementation of UK Earth system models for CMIP6, Journal of Advances in Modeling Earth Systems, 12, e2019MS001 946, 2020.

Shevliakova, E., Pacala, S. W., Malyshev, S., Hurtt, G. C., Milly, P., Caspersen, J. P., Sentman, L. T., Fisk, J. P., Wirth, C., and Crevoisier, C.: Carbon cycling under 300 years of land use change: Importance of the secondary vegetation sink, Global Biogeochemical Cycles, 23, 2009.

Shi, Z., Allison, S. D., He, Y., Levine, P. A., Hoyt, A. M., Beem-Miller, J., Zhu, Q., Wieder, W. R., Trumbore, S., and Randerson, J. T.: The age distribution of global soil carbon inferred from radiocarbon measurements, Nature Geoscience, 13, 555–559, 2020.

Sierra, C. A., Trumbore, S. E., Davidson, E. A., Vicca, S., and Janssens, I.: Sensitivity of decomposition rates of soil organic matter with respect to simultaneous changes in temperature and moisture, Journal of Advances in Modeling Earth Systems, 7, 335–356, 2015.

Swart, N. C., Cole, J. N., Kharin, V. V., Lazare, M., Scinocca, J. F., Gillett, N. P., Anstey, J., Arora, V., Christian, J. R., Hanna, S., et al.: The Canadian earth system model version 5 (CanESM5. 0.3), Geoscientific Model Development, 12, 4823–4873, 2019.

Taylor, K. E., Stouffer, R. J., and Meehl, G. A.: An overview of CMIP5 and the experiment design, Bulletin of the American Meteorological Society, 93, 485–498, 2012.

Todd-Brown, K., Randerson, J., Post, W., Hoffman, F., Tarnocai, C., Schuur, E., and Allison, S.: Causes of variation in soil carbon simulations from CMIP5 Earth system models and comparison with observations, Biogeosciences, 10, 1717–1736, 2013.

Todd-Brown, K., Randerson, J., Hopkins, F., Arora, V., Hajima, T., Jones, C., Shevliakova, E., Tjiputra, J., Volodin, E., Wu, T., et al.: Changes in soil organic carbon storage predicted by Earth system models during the 21st century, Biogeosciences, 11, 2341–2356, 2014.

Todd-Brown, K., Zheng, B., and Crowther, T. W.: Field-warmed soil carbon changes imply high 21st-century<? xmltex\break?> modeling uncertainty, Biogeosciences, 15, 3659–3671, 2018.

Van Gestel, N., Shi, Z., Van Groenigen, K. J., Osenberg, C. W., Andresen, L. C., Dukes, J. S., Hovenden, M. J., Luo, Y., Michelsen, A., Pendall, E., et al.: Predicting soil carbon loss with warming, Nature, 554, E4–E5, 2018.

Varney, R. M., Chadburn, S. E., Friedlingstein, P., Burke, E. J., Koven, C. D., Hugelius, G., and Cox, P. M.: A spatial emergent constraint on the sensitivity of soil carbon turnover to global warming, Nature communications, 11, 1–8, 2020.

Varney, R. M., Chadburn, S. E., Burke, E. J., and Cox, P. M.: Evaluation of soil carbon simulation in CMIP6 Earth system models, Biogeosciences, 19, 4671–4704, https://doi.org/10.5194/bg-19-4671-2022, 2022.

Watanabe, S., Hajima, T., Sudo, K., Nagashima, T., Takemura, T., Okajima, H., Nozawa, T., Kawase, H., Abe, M., Yokohata, T., et al.: MIROC-ESM 2010: Model description and basic results of CMIP5-20c3m experiments, Geoscientific Model Development, 4, 845–872, 2011.

650 Wieder, W. R., Allison, S. D., Davidson, E. A., Georgiou, K., Hararuk, O., He, Y., Hopkins, F., Luo, Y., Smith, M. J., Sulman, B., et al.: Explicitly representing soil microbial processes in Earth system models, Global Biogeochemical Cycles, 29, 1782–1800, 2015a.

Wieder, W. R., Cleveland, C. C., Smith, W. K., and Todd-Brown, K.: Future productivity and carbon storage limited by terrestrial nutrient availability, Nature Geoscience, 8, 441–444, 2015b.

Wiltshire, A. J., Burke, E. J., Chadburn, S. E., Jones, C. D., Cox, P. M., Davies-Barnard, T., Friedlingstein, P., Harper, A. B., Liddicoat,
655 S., Sitch, S., et al.: JULES-CN: a coupled terrestrial carbon–nitrogen scheme (JULES vn5. 1), Geoscientific Model Development, 14, 2161–2186, 2021.

Wu, T., Lu, Y., Fang, Y., Xin, X., Li, L., Li, W., Jie, W., Zhang, J., Liu, Y., Zhang, L., et al.: The Beijing Climate Center climate system model (BCC-CSM): The main progress from CMIP5 to CMIP6, Geoscientific Model Development, 12, 1573–1600, 2019.

Yue, X. and Unger, N.: The Yale Interactive terrestrial Biosphere model version 1.0: description, evaluation and implementation into NASA
660 GISS ModelE2, Geoscientific Model Development, 8, 2399–2417, 2015.

Zhao, M., Golaz, J.-C., Held, I., Guo, H., Balaji, V., Benson, R., Chen, J.-H., Chen, X., Donner, L., Dunne, J., et al.: The GFDL global atmosphere and land model AM4. 0/LM4. 0: 2. Model description, sensitivity studies, and tuning strategies, Journal of Advances in Modeling Earth Systems, 10, 735–769, 2018.

Ziehn, T., Chamberlain, M. A., Law, R. M., Lenton, A., Bodman, R. W., Dix, M., Stevens, L., Wang, Y.-P., and Srbinovsky, J.: The Australian
665 Earth System Model: ACCESS-ESM1. 5, Journal of Southern Hemisphere Earth Systems Science, 70, 193–214, 2020.
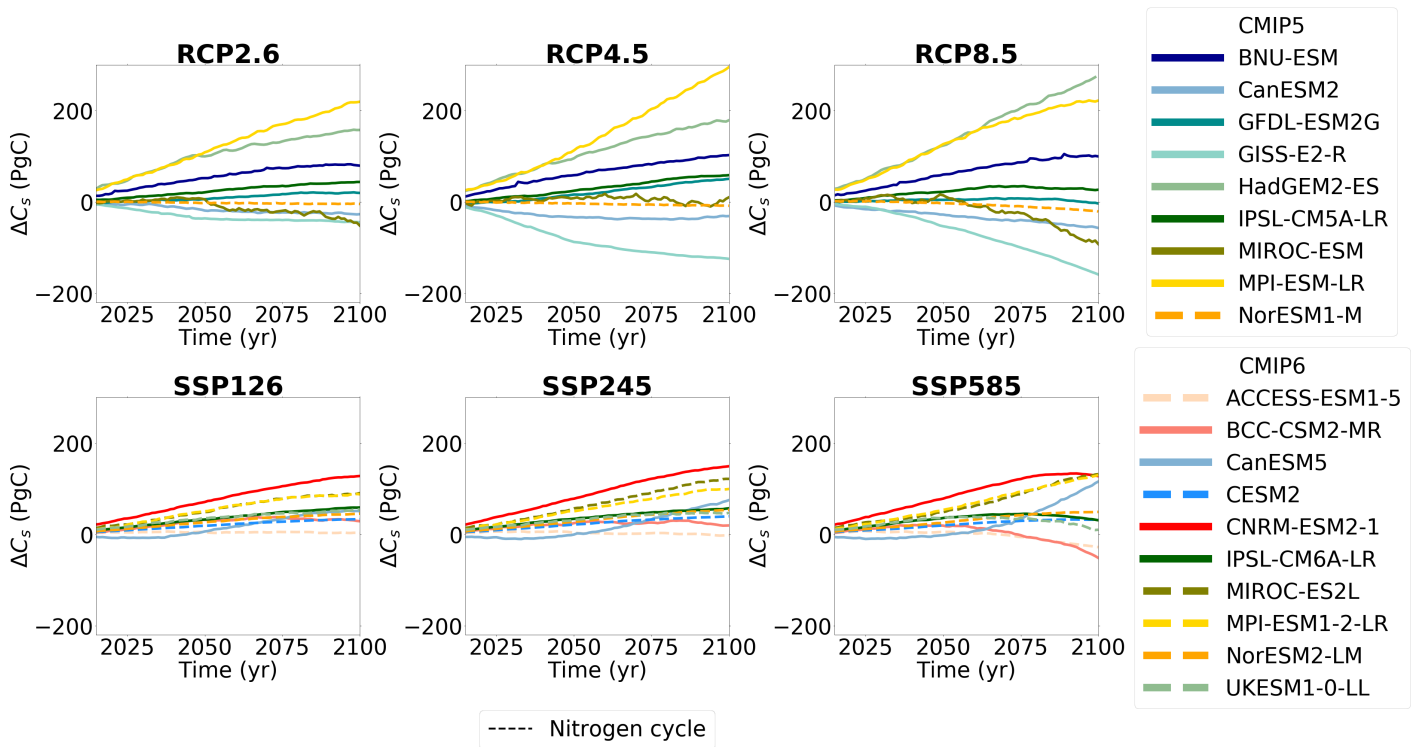
**Figure 1.** Projected future change in soil carbon ($\Delta C_s$) in CMIP5 (top row) and CMIP6 (bottom row) ESMs, for future climate scenarios *RCP2.6* and *SSP126*, *RCP4.5* and *SSP245*, *RCP8.5* and *SSP585*, respectively. The dashed lines represent ESMs which include the representation of interactive nitrogen in these simulations.
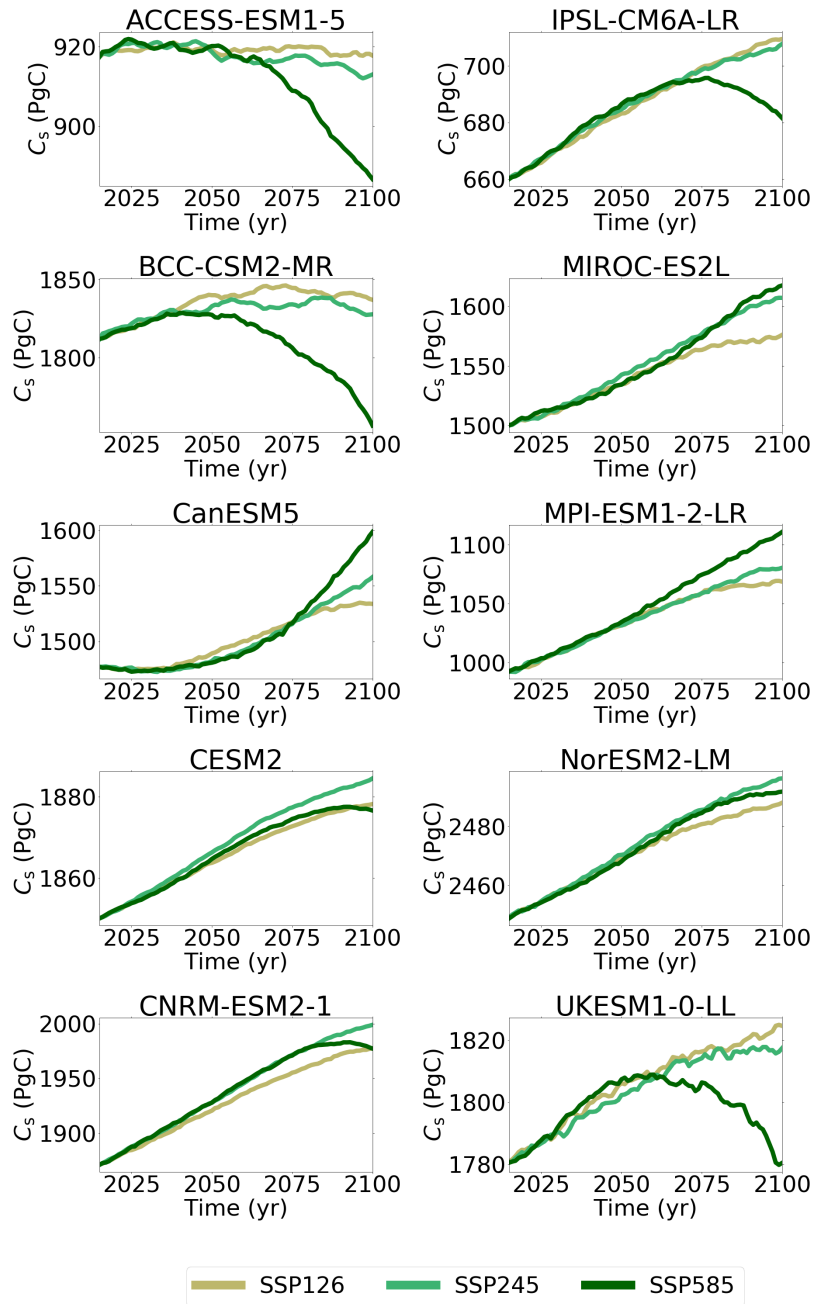
**Figure 2.** Timeseries of projected future soil carbon ($C_s$) in CMIP6 ESMs for future climate scenarios *SSP126*, *SSP245*, *SSP585*.
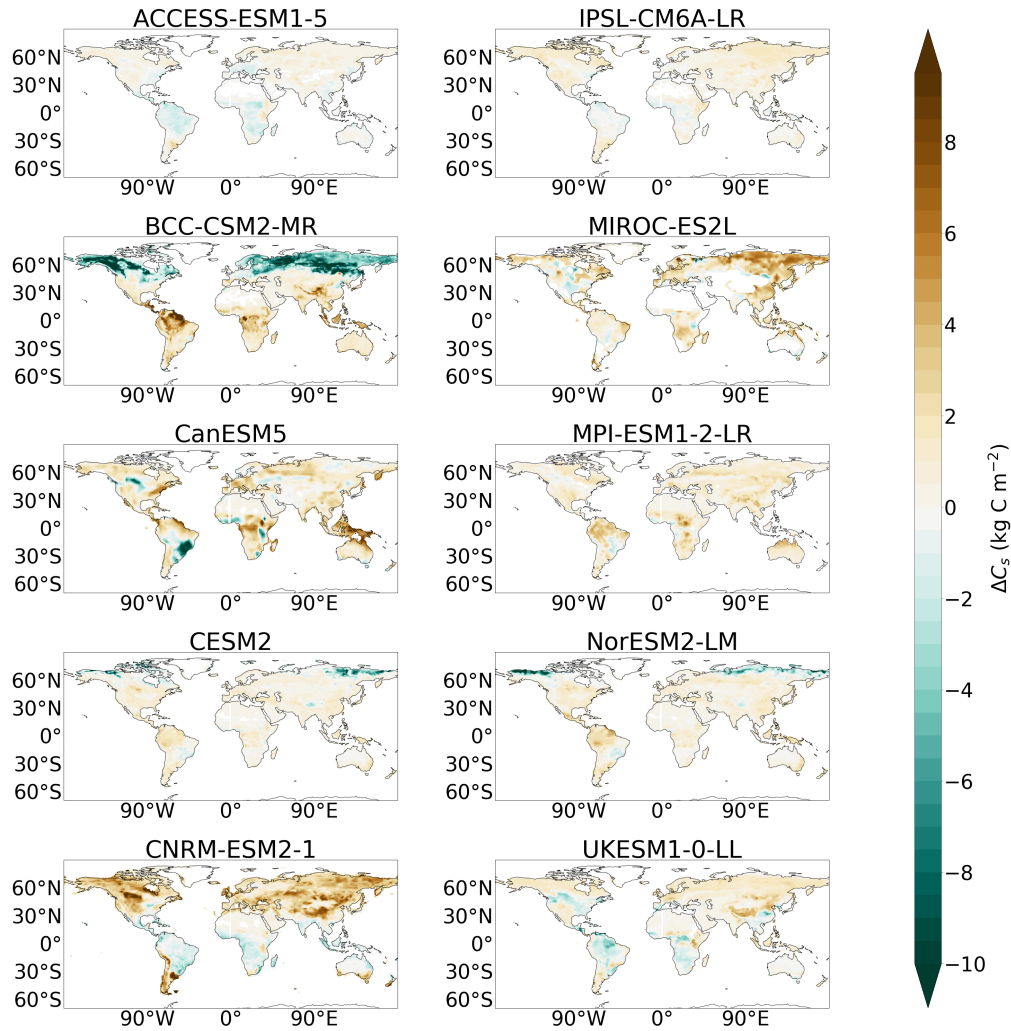
**Figure 3.** Map plots showing the change in soil carbon ($\Delta C_s$) in *SSP585* for each CMIP6 ESM.
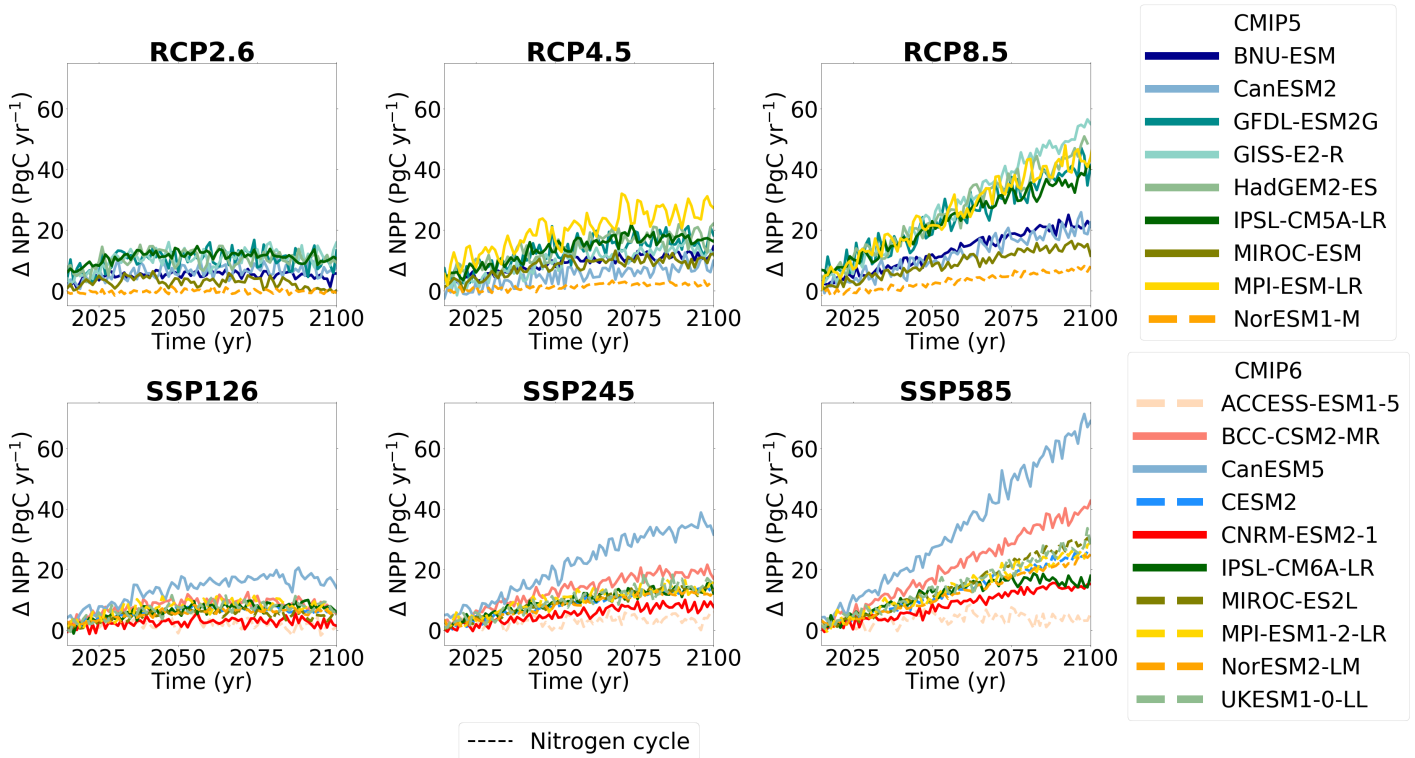
**Figure 4.** Projected future change in Net Primary Production (ΔNPP) in CMIP5 (top row) and CMIP6 (bottom row) ESMs, for future climate scenarios *RCP2.6* and *SSP126*, *RCP4.5* and *SSP245*, *RCP8.5* and *SSP585*, respectively. The dashed lines represent ESMs which include the representation of interactive nitrogen in these simulations.
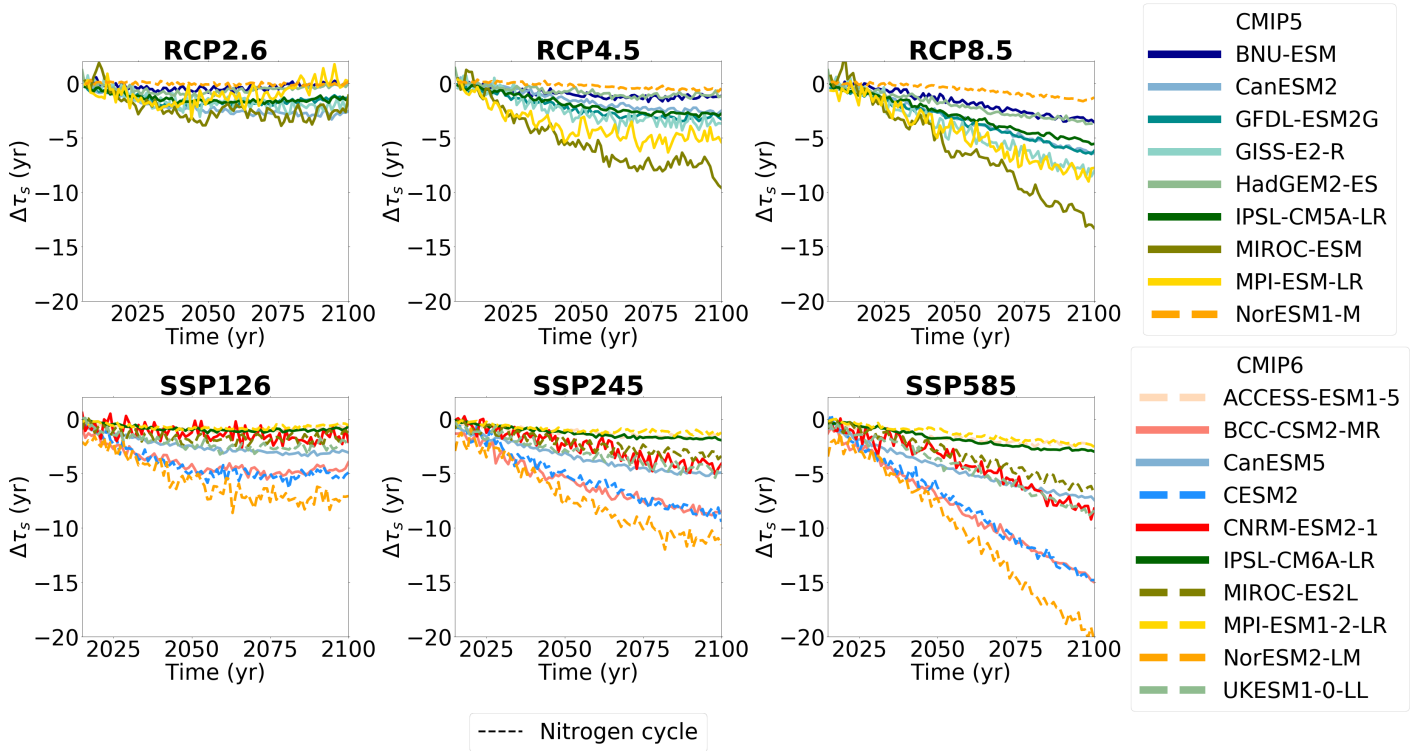
**Figure 5.** Projected future change in soil carbon turnover time ($\Delta\tau_s$) in CMIP5 (top row) and CMIP6 (bottom row) ESMs, for future climate scenarios *RCP2.6* and *SSP126*, *RCP4.5* and *SSP245*, *RCP8.5* and *SSP585*, respectively. The dashed lines represent ESMs which include the representation of interactive nitrogen in these simulations.
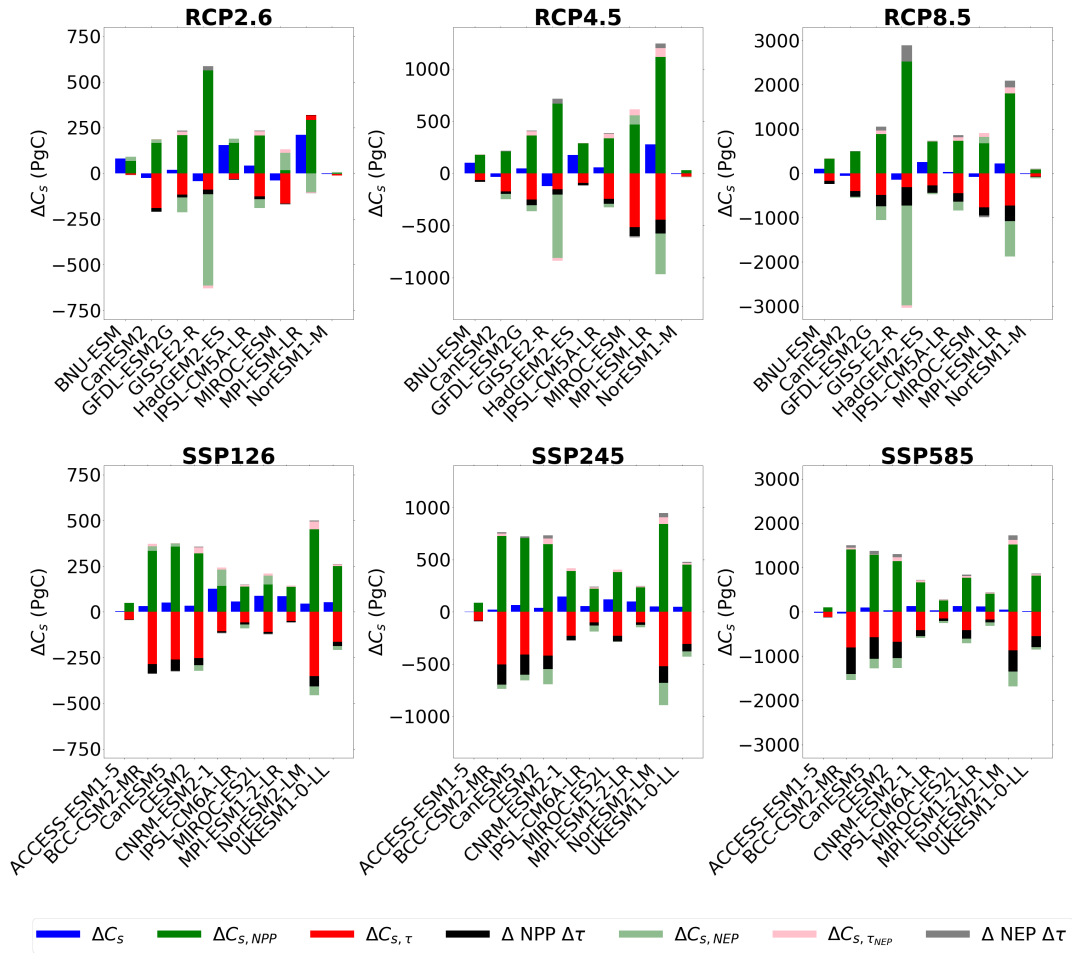
**Figure 6.** A bar chart showing the contributions of NPP and $\tau_s$ to end of $21^{\text{st}}$ century changes in soil carbon ($\Delta C_s$) in CMIP5 (top row) and CMIP6 (bottom row) ESMs, for future scenarios: *RCP2.6* and *SSP126*, *RCP4.5* and *SSP245*, *RCP8.5* and *SSP585*, respectively. The included terms are: the linear term representing changes in soil carbon due to the changes in NPP ($\Delta C_{s,NPP}$), the linear term representing changes in soil carbon due to the changes in $\tau_s$ ($\Delta C_{s,\tau}$), the non-linear term ($\Delta \text{NPP} \Delta \tau_s$), and then additional terms to account for the non-equilibrium climate in 2100 ($\Delta C_{s,NEP}$, $\Delta C_{s,\tau_{NEP}}$, and $\Delta \text{NEP} \Delta \tau_s$).
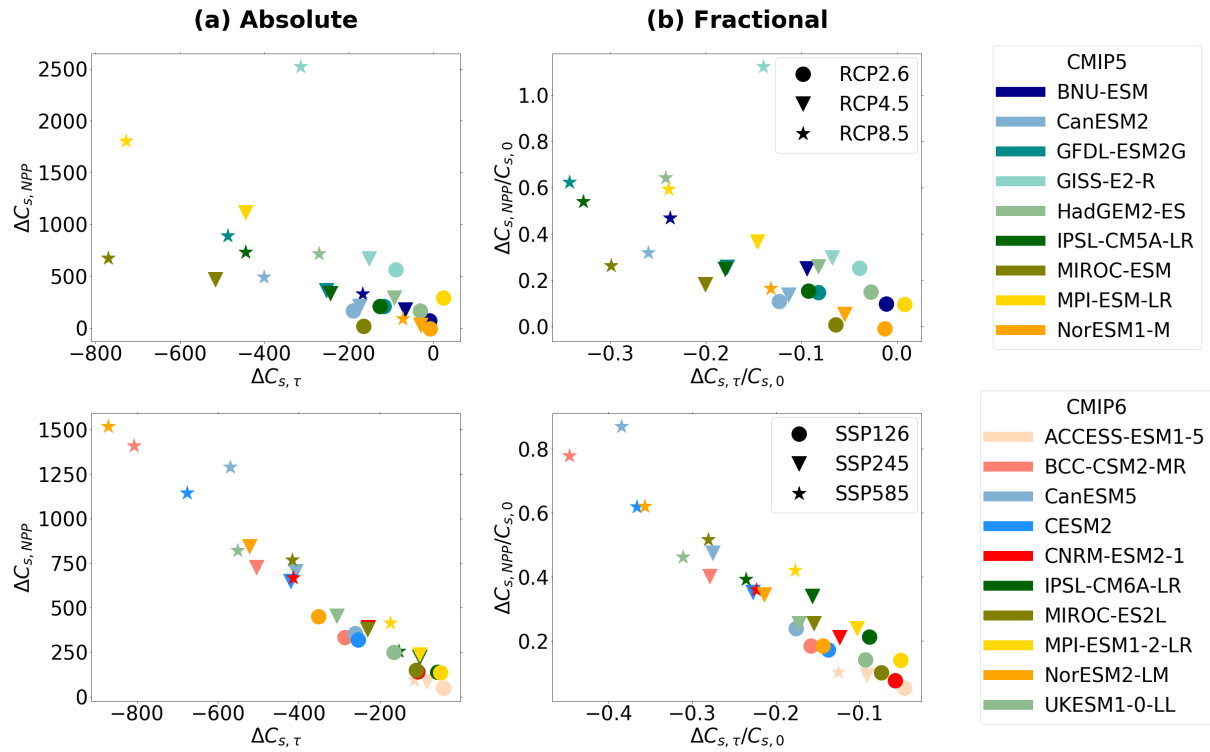
**Figure 7.** Scatter plot comparing the relationship between $\Delta C_{s,NPP}$ and $\Delta C_{s,\tau}$ for CMIP5 (top row) and CMIP6 (bottom row) ESMs in future scenarios *RCP2.6* and *SSP126*, *RCP4.5* and *SSP245*, *RCP8.5* and *SSP585*, respectively, for (a) absolute changes, and (b) fractional changes.
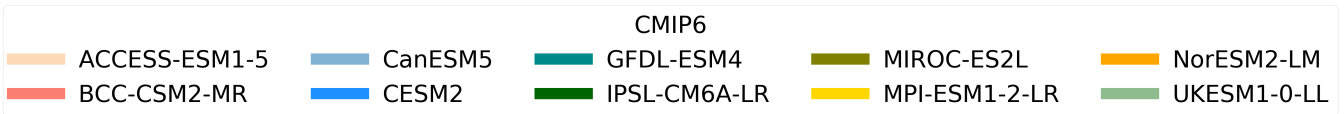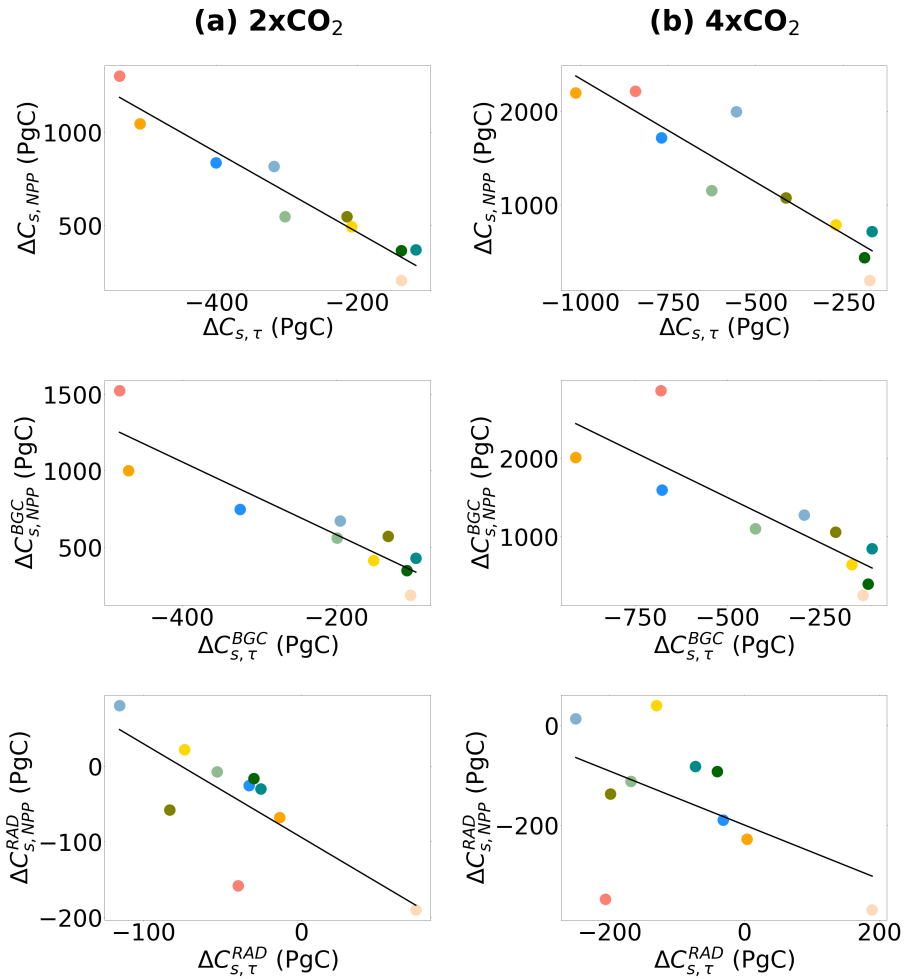
**Figure 8.** Scatter plots showing the relationship between $\Delta C_{s,NPP}$ and $\Delta C_{s,\tau}$ for each CMIP6 ESM, in the *full* 1% $CO_2$ simulation (top row), *BGC* simulation (middle row) and *RAD* simulation (bottom row), for (a) 2x$CO_2$ and (b) 4x$CO_2$.
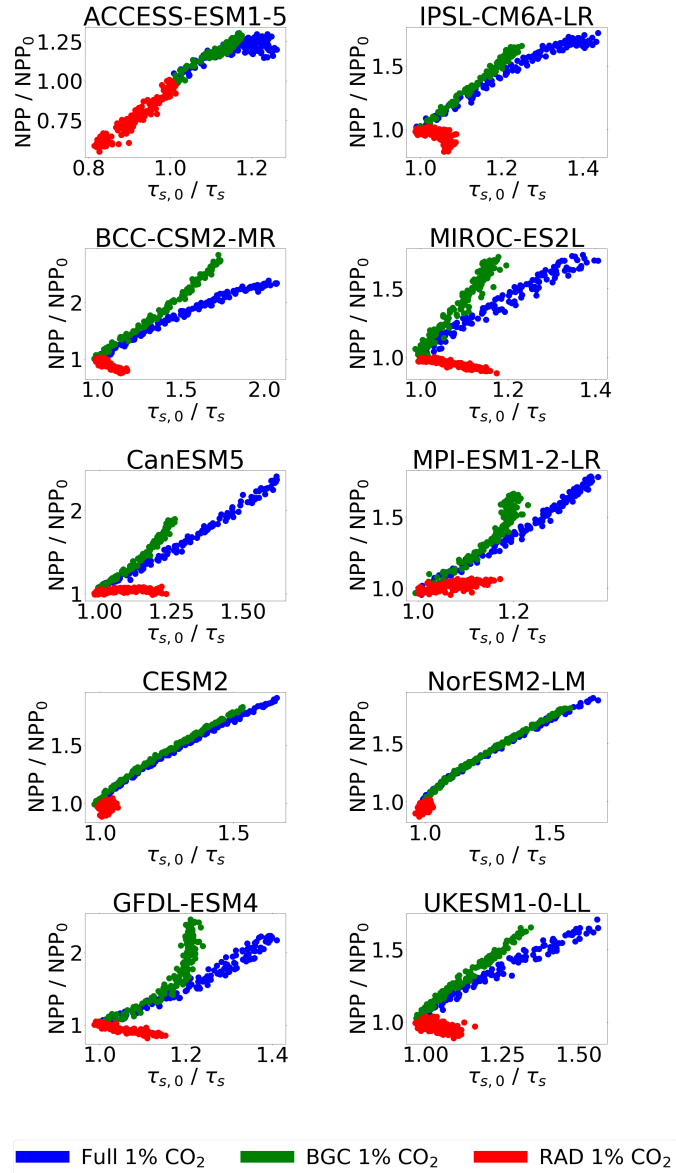
**Figure 9.** Scatter plots showing the correlation between $NPP/NPP_0$ and $\tau_{s,0}/\tau_s$ for each CMIP6 ESM, in the *full* 1% $CO_2$ simulation (blue) and the *BGC* simulation (green), up to 4x$CO_2$.
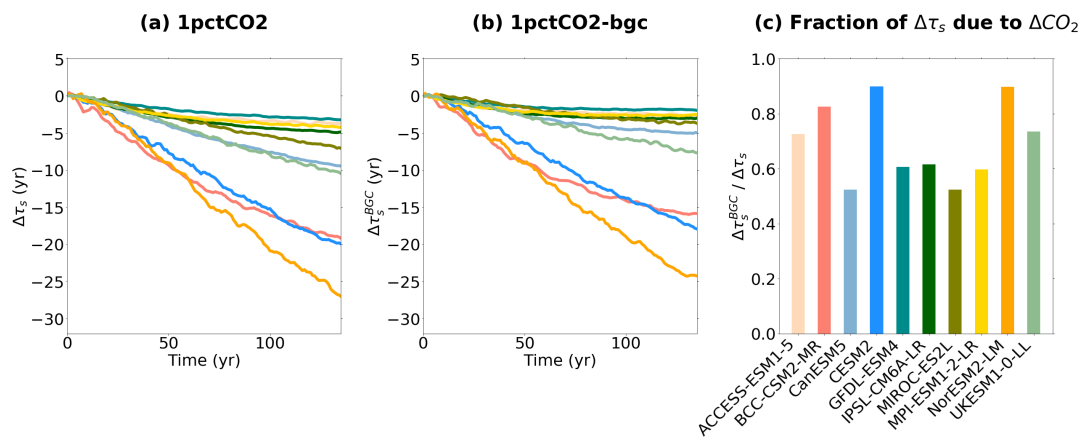
**Figure 10.** Changes in soil carbon turnover ($\Delta\tau_s$) in C4MIP runs for the CMIP6 ESMs, with and without direct climate effects on $\tau_s$. (a) timeseries of $\Delta\tau_s$ in *full* 1% $CO_2$ simulation (climate and $CO_2$ changes), (b) timeseries of $\Delta\tau_s$ in *BGC* simulation ($CO_2$ changes only), and (c) bar chart showing the fraction of total $\Delta\tau_s$ due to the changes in $CO_2$ at 4x$CO_2$ for each model.
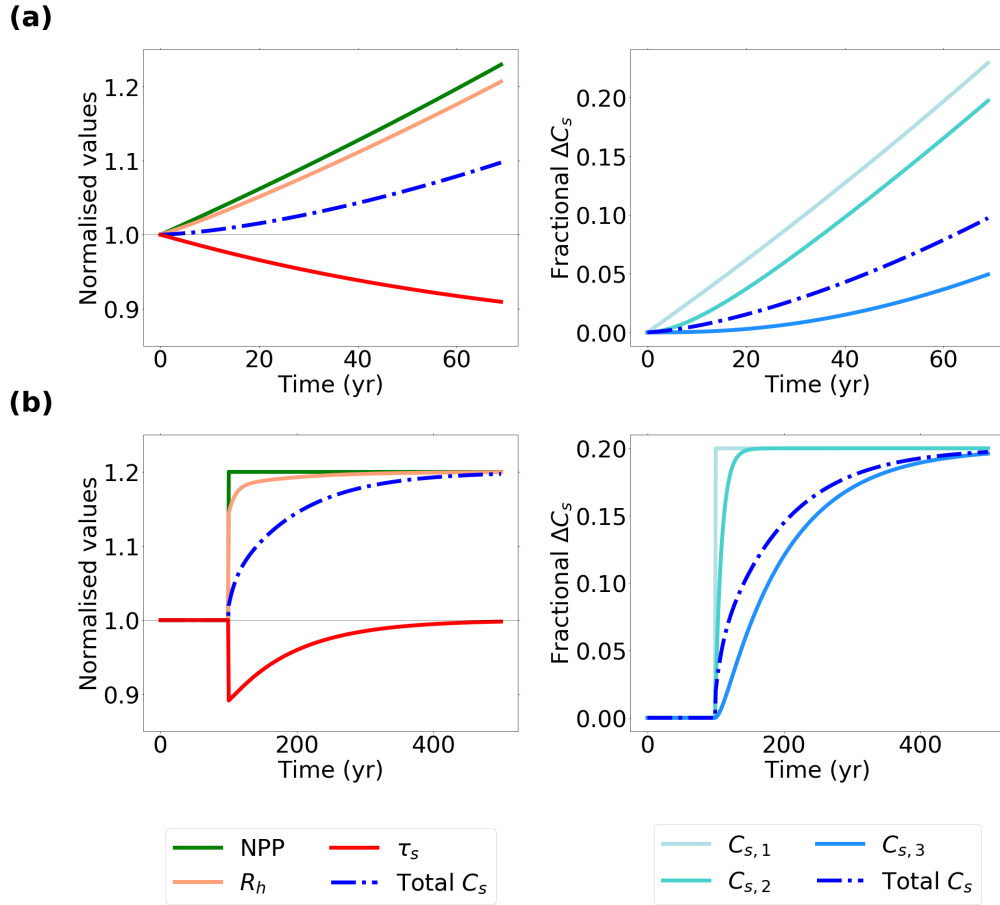
**Figure 11.** Timeseries plot showing the results from the simple three-box model. (a) For normalised changes in NPP, $R_h$, $\tau_s$ and $C_s$ and fractional change in each of the 3 soil carbon boxes and in the total soil carbon (recreation of Fig. 12 in Koven et al. (2015)). (b) For an abrupt change in global NPP, from 50 PgC yr$^{-1}$ to 70 PgC yr$^{-1}$ at year 100.
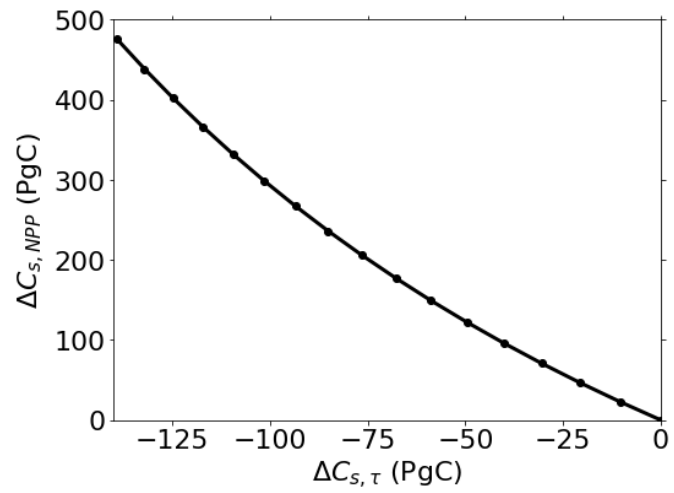
**Figure 12.** Relationship between $\Delta C_{s,NPP}$ and $\Delta C_{s,\tau}$ derived from the three-box model. Each dot represents the results at the end of a 70 year run with a different assumed rate of increase of NPP ($\sim 0.0\%$ to $0.8\%$ per year in increments of $0.05\%$).

**Table 1.** The CMIP5 and CMIP6 Earth system models included in this study and the relevant features of associated land carbon cycle components: simulation of interactive nitrogen, number of live carbon pools and the number of dead soil carbon pools (Varney et al., 2022; Arora et al., 2013, 2020).

| Earth System Model | Nitrogen cycle | No. of live carbon pools | No. of dead carbon pools | References |
|---|---|---|---|---|
| BNU-ESM | No | - | - | Ji et al. (2014); Dai et al. (2003) |
| CanESM2 | No | 3 | 2 | Arora et al. (2009); Arora and Boer (2010) |
| GFDL-ESM2G | No | 8 | 2 | Dunne et al. (2012, 2013); Shevliakova et al. (2009) |
| GISS-E2-R | No | 7 | 5 | Schmidt et al. (2014); Yue and Unger (2015) |
| HadGEM2-ES | No | 3 | 4 | Jones et al. (2011); Best et al. (2011): Clark et al. (2011) |
| IPSL-CM5A-LR | No | - | 7 | Dufresne et al. (2013); Krinner et al. (2005) |
| MIROC-ESM | No | 4 | 2 | Watanabe et al. (2011); Ito and Oikawa (2002); Sato et al. (2007) |
| MPI-ESM-LR | No | 4 | 2 | Raddatz et al. (2007); Knorr (2000) |
| NorESM1-M | Yes | 13 | 7 | Bentsen et al. (2013); Iversen et al. (2013); Lawrence et al. (2011) |
| ACCESS-ESM1.5 | Yes | 3 | 6 | Ziehn et al. (2020); Haverd et al. (2018); |
| BCC-CSM2-MR | No | 3 | 8 | Wu et al. (2019); Ji et al. (2008) |
| CanESM5 | No | 3 | 2 | Swart et al. (2019); Melton et al. (2020); Seiler et al. (2021) |
| CESM2 | Yes | 22 | 7 | Danabasoglu et al. (2020); Lawrence et al. (2019) |
| CNRM-ESM2-1 | No | 6 | 7 | Séférian et al. (2019); Delire et al. (2020) |
| GFDL-ESM4 | No | 6 | 4 | Dunne et al. (2020); Zhao et al. (2018) |
| IPSL-CM6A-LR | No | 8 | 3 | Boucher et al. (2020); Cheruy et al. (2020); Guimberteau et al. (2018) |
| MIROC-ES2L | Yes | 3 | 6 | Hajima et al. (2020); Ito and Oikawa (2002) |
| MPI-ESM1.2-LR | Yes | 3 | 18 | Mauritsen et al. (2019); Goll et al. (2017); Goll et al. (2015) |
| NorESM2-LM | Yes | 22 | 7 | Seland et al. (2020); Lawrence et al. (2019) |
| UKESM1-0-LL | Yes | 3 | 4 | Sellar et al. (2020); Wiltshire et al. (2021) |

**Table 2.** Table presenting the absolute (PgC) and relative (%) change in 21$^{st}$ century soil carbon ($\Delta C_s$) for each CMIP6 model and the ensemble mean ± standard deviation, for each future SSP scenario.

| Earth System Model | Absolute $\Delta C_s$ (PgC) | | | Relative $\Delta C_s$ (%) | | |
|---|---|---|---|---|---|---|
| | SSP126 | SSP245 | SSP585 | SSP126 | SSP245 | SSP585 |
| ACCESS-ESM1.5 | 3.44 | -0.98 | -23.4 | 0.38 | -0.108 | -2.55 |
| BCC-CSM2-MR | 31.8 | 22.3 | -35.2 | 1.76 | 1.23 | -1.95 |
| CanESM5 | 50.6 | 66.7 | 97.7 | 3.41 | 4.49 | 6.59 |
| CESM2 | 32.7 | 38.3 | 32.4 | 1.77 | 2.08 | 1.76 |
| CNRM-ESM2-1 | 126 | 145 | 132 | 6.79 | 7.85 | 7.11 |
| IPSL-CM6A-LR | 57.6 | 55.0 | 35.5 | 8.86 | 8.45 | 5.46 |
| MIROC-ES2L | 87.3 | 118 | 126 | 5.88 | 7.94 | 8.5 |
| MPI-ESM1-2-LR | 86.2 | 97.9 | 123 | 8.79 | 9.98 | 12.5 |
| NorESM2-LM | 44.1 | 52.0 | 48.7 | 1.81 | 2.13 | 1.99 |
| UKESM1-0-LL | 52.3 | 46.9 | 17.5 | 2.96 | 2.65 | 0.988 |
| Ensemble mean | 55.4 | 58.3 | 50.3 | 4.53 | 4.24 | 3.67 |
| ± standard deviation | ± 31.8 | ± 44.3 | ± 57.8 | ± 2.95 | ± 3.51 | ± 4.50 |

**Table 3.** Table presenting the change in 21$^{\text{st}}$ century NPP and $\tau_s$ for each CMIP6 model and the ensemble mean $\pm$ standard deviation, for each future SSP scenario.

| Earth System Model | $\Delta$NPP (PgC yr$^{-1}$) | | | $\Delta\tau_s$ (yr) | | |
|---|---|---|---|---|---|---|
| | SSP126 | SSP245 | SSP585 | SSP126 | SSP245 | SSP585 |
| ACCESS-ESM1.5 | 1.66 | 3.58 | 4.07 | -0.828 | -1.69 | -2.35 |
| BCC-CSM2-MR | 8.37 | 19.7 | 39.4 | -4.53 | -8.52 | -14.0 |
| CanESM5 | 17.4 | 35.4 | 65.8 | -3.09 | -5.01 | -7.10 |
| CESM2 | 6.46 | 13.7 | 24.5 | -5.05 | -8.63 | -14.1 |
| CNRM-ESM2-1 | 2.28 | 7.96 | 14.3 | -1.624 | -4.19 | -8.05 |
| IPSL-CM6A-LR | 8.40 | 13.9 | 16.2 | -0.938 | -1.81 | -2.83 |
| MIROC-ES2L | 4.90 | 13.9 | 29.0 | -1.52 | -3.37 | -6.23 |
| MPI-ESM1-2-LR | 7.84 | 14.3 | 25.9 | -0.555 | -1.27 | -2.30 |
| NorESM2-LM | 6.33 | 12.6 | 23.3 | -7.16 | -11.0 | -18.9 |
| UKESM1-0-LL | 8.08 | 15.2 | 28.1 | -2.37 | -4.52 | -8.25 |
| Ensemble mean | 7.44 | 13.6 | 24.6 | -2.30 | -4.55 | -7.65 |
| $\pm$ standard deviation | $\pm$ 4.01 | $\pm$ 8.71 | $\pm$ 16.9 | $\pm$ 2.047 | $\pm$ 3.35 | $\pm$ 5.65 |
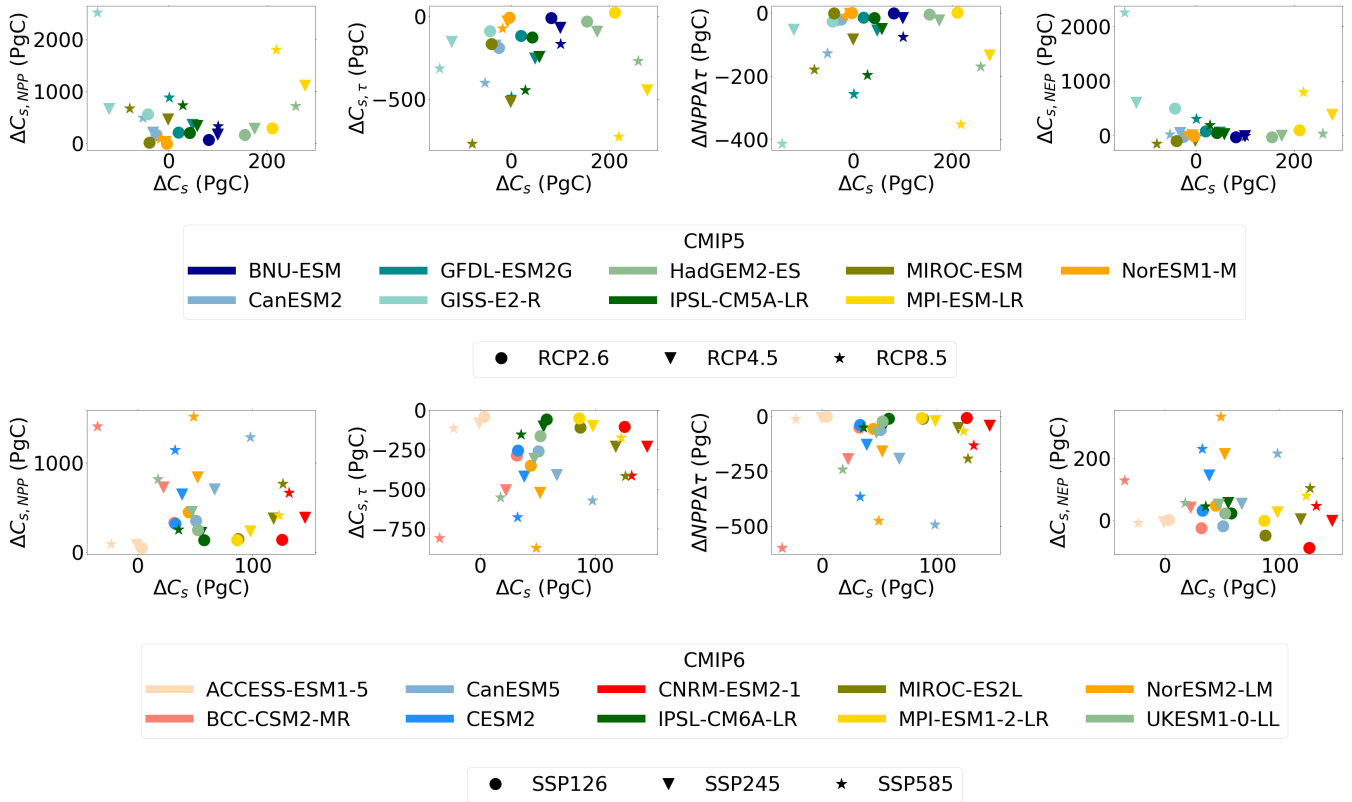
**Figure A1.** Scatter plot comparing the relationship between $\Delta C_{s,NPP}$, $\Delta C_{s,\tau}$, $\Delta \text{NPP} \Delta \tau_s$, and $\Delta C_{s,\tau_{NEP}}$, each against $\Delta C_s$, for CMIP5 (top row) and CMIP6 (bottom row) ESMs, for future scenarios *SSP126* and *RCP2.6*, *SSP245* and *RCP4.5*, *SSP585* and *RCP8.5*.
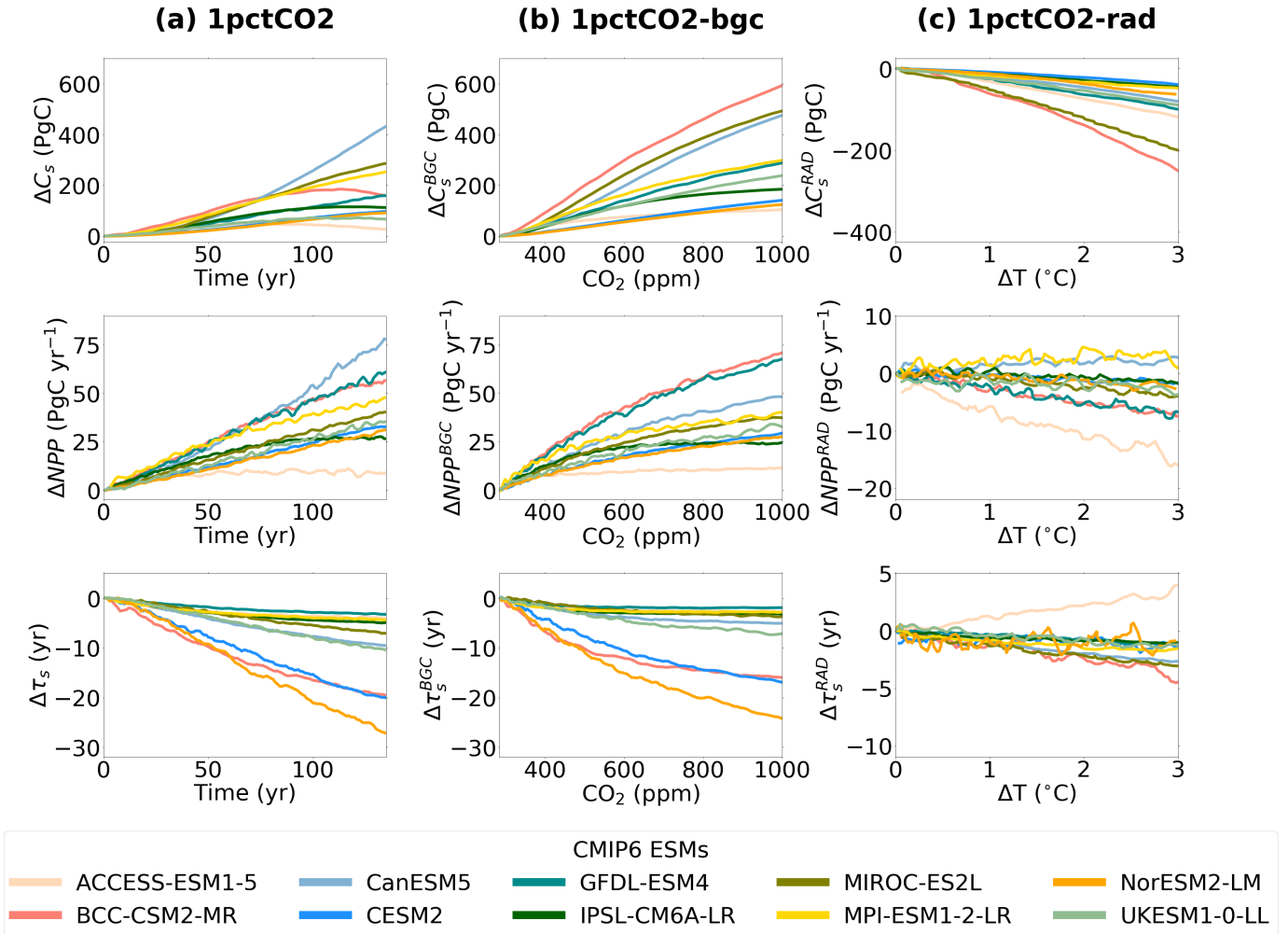
**Figure A2.** Timeseries of projected changes in Soil carbon ($\Delta C_s$, top row) Net Primary Productivity ($\Delta$NPP, middle row), and soil carbon turnover time ($\Delta \tau_s$, bottom row) in CMIP6 ESMs for the idealised simulations 1% $CO_2$ (left column), biogeochemically coupled 1% $CO_2$ (*BGC*, middle column) and radiatively coupled 1% $CO_2$ (*RAD*, right column).

**Table A1.** Table presenting the absolute (PgC) and relative (%) change in $21^{st}$ century soil carbon for each CMIP5 model and the ensemble mean ± standard deviation, for each future RCP scenario.

| Earth System Model | Absolute $\Delta C_s$ (PgC) | | | Relative $\Delta C_s$ (%) | | |
|---|---|---|---|---|---|---|
| | RCP2.6 | RCP4.5 | RCP8.5 | RCP2.6 | RCP4.5 | RCP8.5 |
| BNU-ESM | 81.4 | 99.7 | 100 | 11.6 | 14.2 | 14.3 |
| CanESM2 | -25.4 | -32.7 | -53.5 | -1.65 | -2.12 | -3.47 |
| GFDL-ESM2G | 19.9 | 47.9 | 0.278 | 1.40 | 3.37 | 0.020 |
| GISS-E2-R | -43.1 | -122 | -146 | -1.92 | -5.43 | -6.50 |
| HadGEM2-ES | 154 | 174 | 258 | 13.9 | 15.6 | 23.2 |
| IPSL-CM5A-LR | 42.5 | 57.1 | 28.4 | 3.14 | 4.22 | 2.10 |
| MIROC-ESM | -39.9 | -1.53 | -80.0 | -1.55 | -0.059 | -3.11 |
| MPI-ESM-LR | 211 | 277 | 219 | 6.94 | 9.09 | 7.19 |
| NorESM1-M | -3.94 | -7.60 | -17.7 | -0.723 | -1.40 | -3.26 |
| Ensemble mean | 44.1 | 54.7 | 34.3 | 3.45 | 4.17 | 3.38 |
| ± standard deviation | ± 84.2 | ± 111 | ± 127 | ± 5.66 | ± 6.97 | ± 9.24 |

**Table A2.** Table presenting the change in 21$^{\text{st}}$ century NPP and $\tau_s$ for each CMIP5 model and the ensemble mean $\pm$ standard deviation, for each future RCP scenario.

| Earth System Model | $\Delta$NPP (PgC) | | | $\Delta\tau_s$ (yr) | | |
|---|---|---|---|---|---|---|
| | RCP2.6 | RCP4.5 | RCP8.5 | RCP2.6 | RCP4.5 | RCP8.5 |
| BNU-ESM | 4.52 | 11.7 | 21.9 | -0.165 | -1.36 | -3.42 |
| CanESM2 | 6.94 | 8.73 | 20.4 | -2.95 | -2.71 | -6.23 |
| GFDL-ESM2G | 9.47 | 16.4 | 40.13 | -1.53 | -3.31 | -6.38 |
| GISS-E2-R | 11.5 | 13.6 | 51.4 | -2.26 | -3.88 | -8.03 |
| HadGEM2-ES | 10.4 | 18.2 | 45.5 | -0.40 | -1.24 | -3.66 |
| IPSL-CM5A-LR | 10.4 | 16.9 | 37.0 | -1.50 | -2.91 | -5.31 |
| MIROC-ESM | 0.350 | 9.98 | 14.4 | -2.66 | -8.32 | -12.4 |
| MPI-ESM-LR | - | 26.6 | 43.0 | -0.280 | -5.00 | -8.17 |
| NorESM1-M | -0.388 | 2.25 | 6.94 | -0.151 | -0.645 | -1.55 |
| Ensemble mean | 5.32 | 12.4 | 28.1 | -1.26 | -3.26 | -6.13 |
| $\pm$ standard deviation | $\pm$ 4.74 | $\pm$ 7.42 | $\pm$ 16.8 | $\pm$ 1.13 | $\pm$ 2.21 | $\pm$ 3.03 |